



PERGAMON

Available online at [www.sciencedirect.com](http://www.sciencedirect.com)

SCIENCE @ DIRECT®

Deep-Sea Research I 50 (2003) 23–52

DEEP-SEA RESEARCH  
PART I

[www.elsevier.com/locate/dsr](http://www.elsevier.com/locate/dsr)

# Is Labrador Sea Water formed in the Irminger basin?

Robert S. Pickart<sup>a,\*</sup>, Fiammetta Straneo<sup>a</sup>, G.W.K. Moore<sup>b</sup>

<sup>a</sup>Physical Oceanography Department, Woods Hole Oceanographic Institution, Clark 355B Ms21, Woods Hole, MA 02543, USA

<sup>b</sup>University of Toronto, USA

Received 1 March 2002; accepted 4 October 2002

## Abstract

Present day thinking contends that Labrador Sea Water (LSW), one of the major watermasses of the North Atlantic, is formed exclusively in the Labrador basin via deep wintertime convection. It is argued herein that LSW is likely formed at a second location—the southwest Irminger Sea. We base this on two pieces of evidence: (1) tracer observations in the western subpolar gyre are inconsistent with a single source and (2) the combination of oceanic and atmospheric conditions that lead to convection in the Labrador Sea is present as well east of Greenland. Hydrographic data (both recent and climatological) are used, in conjunction with an advective–diffusive numerical model, to demonstrate that the spatial distribution of LSW and its inferred spreading rate are inconsistent with a Labrador Sea-only source. The spreading would have to be unrealistically fast, and could not produce the extrema of LSW properties observed in the Irminger basin. At the same time, the set of conditions necessary for deep convection to occur—a preconditioned water column, cyclonic circulation, and strong air–sea buoyancy fluxes—are satisfied in the Irminger Sea. Using observed parameters, a mixed-layer model shows that, under the right conditions, overturning can occur in the Irminger Sea to a depth of 1500–2000 m, forming LSW.

© 2003 Elsevier Science Ltd. All rights reserved.

## 1. Introduction

It is now well established that deep convection occurs at only a few special sites in the world ocean, where atmospheric forcing conspires with the oceanographic circulation and preconditioning to cause the necessary conditions for overturning. One of these sites is the Labrador Sea, where a mid-depth water mass is formed known as Labrador Sea Water (LSW, e.g. Lazier, 1973). This water mass influences a large area of the North Atlantic and is easily detected by its cold, fresh signature, as well as its anomalously low

potential vorticity (PV)<sup>1</sup> and high concentration of anthropogenic tracers (Talley and McCartney, 1982; Smethie et al., 2000). The large-scale impacts of LSW formation are substantial and varied. For instance, LSW contributes significantly to the meridional overturning circulation (Schmitz and McCartney, 1993), global heat flux (Talley, 2000), and modification of the Nordic overflow waters (e.g. McCartney, 1992). It dictates to a large degree the stratification of the interior North Atlantic and its boundary currents. The PV signature of LSW has even been implicated in

\*Corresponding author.

E-mail address: [rpickart@whoi.edu](mailto:rpickart@whoi.edu) (R.S. Pickart).

<sup>1</sup>Planetary potential vorticity is defined as  $PV = (f/\rho)(\partial\rho/\partial z)$ , where  $f$  is the Coriolis parameter,  $\rho$  the density, and  $z$  the depth (positive upwards).

the stability of the Gulf Stream system (Spall, 1996).

The common belief is that LSW is formed entirely within the Labrador Basin via deep convection, which, under the right circumstances, can extend to 2 km (Lazier et al., 2002). After formation, the newly ventilated water spreads laterally from the basin into the North Atlantic (e.g. Talley and McCartney, 1982; Harvey and Arhan, 1988; Rhein et al., 2002). Numerous investigators have identified and mapped LSW in the “far-field”, and have estimated formation rates and spreading times. Formation estimates range from 6–7 Sv (Smethie and Fine, 2000; Rhein et al., 2002) to 3–4 Sv (Wright, 1972; Clarke and Gascard, 1983) to as little as 1–2 Sv (Worthington, 1976; Speer et al., 1995; Spall and Pickart, 2001). LSW spreading rates have been calculated a variety of ways. For example, Weiss et al. (1985) and Smethie et al. (2000) used the chlorofluorocarbon (CFC) ratio to estimate the time of formation of recently ventilated mid-depth waters in the subtropical North Atlantic. Top et al. (1987) computed the tritium–helium age of LSW found in the subpolar North Atlantic. Read and Gould (1992), Ellett (1993), and Cunningham and Haine (1995) deduced transit times of LSW into the far eastern North Atlantic by comparing observed salinities to the source function of LSW in the Labrador basin. These studies have produced fairly slow spreading rates, on the order of 1.5 cm/s along the western boundary and 0.5 cm/s in the interior.

Recently, however, LSW transit times estimated for the interior subpolar North Atlantic have been significantly faster than this (Sy et al., 1997; Koltermann et al., 1999). Sy et al. (1997) computed an advective speed three to four times larger for LSW progressing into the eastern North Atlantic. More surprisingly, their estimated lag time for LSW to reach the Irminger basin was less than a year, implying an advective speed of 4–5 cm/s. Sy et al. (1997) do not suggest a recent change in the circulation of the North Atlantic, but instead call into question the validity of some of the earlier studies.

These new estimates are based on hydrographic data collected in the mid 1990s, during which time

the North Atlantic Oscillation (NAO) was in an extended “high phase”. The NAO is the dominant mode of atmospheric variability over the North Atlantic (Rogers, 1990) and is represented by an index denoting the wintertime sea level pressure difference between Iceland and the Azores (Hurrell, 1995). A high NAO index means increased storminess and stronger air–sea buoyancy flux over the Labrador Sea, and hence a greater likelihood for convection there (Dickson et al., 1996). The mid-1990s was also the time of the Atlantic component of the World Ocean Circulation Experiment (WOCE), and cruises throughout the North Atlantic detected large amounts of newly ventilated LSW.

A common thread in all of these studies is the assumption that the sole source of LSW is the Labrador basin. In this paper we argue that the formation of LSW is not restricted to the Labrador Sea. In particular, we aim to demonstrate that a significant portion of this water mass is formed by deep convection in the western Irminger Sea, when the atmospheric forcing is strong enough. This can be thought of as an alternate hypothesis for the sudden and conspicuous appearance of newly ventilated LSW in the Irminger basin in the 1990s, and part of the reason why so much LSW was seen in the eastern North Atlantic during WOCE. Deep convection east of Greenland is not a new concept—for instance Nansen (1912) argued that deep water was formed in the Irminger Sea—but present day thinking, based on modern data, has tended to discount this notion. However, as detailed below, there is strong circumstantial evidence from newly collected data that deep convection must at times take place in the western Irminger Sea. If this is true, it will alter our thinking on a variety of issues regarding mid-depth ventilation of the North Atlantic, including water mass formation and spreading rates.

Our approach in this paper will be first to discuss the “Labrador Sea–centric” point of view, i.e. the notion that all LSW is formed in the Labrador Basin and subsequently spreads outwards. We will reveal several inconsistencies in this viewpoint using recently collected data. Then we present a series of arguments outlining why convection in the Irminger Sea is likely. This

includes discussion of the oceanographic preconditioning, circulation, and atmospheric forcing in the Irminger basin. Finally, an advective–diffusive model is used to investigate the spreading of LSW, which, when compared to observed tracer distributions, reinforces the notion that local formation must occur in the Irminger Sea.

## 2. Remote spreading of Labrador Sea Water

### 2.1. Present-day notion

LSW is formed in the western portion of the Labrador Sea (Clarke and Gascard, 1983; Wallace and Lazier, 1988; Pickart et al., 2002a), due in part to the cold wintertime northwesterly winds associated with low-pressure systems that traverse the area. McCartney and Talley (1982) argue that LSW is the end-product of a succession of “mode waters” formed along the cyclonic path of the subpolar gyre via air–sea interaction, beginning offshore of the North Atlantic Current and ending in the Labrador Sea. Talley (1999) recently revised this scheme, emphasizing the distinction of mode waters east and west of the subpolar front, and noting the intensification of the mode water signature near lateral boundaries. Once formed, LSW (the deepest and densest mode water) then spreads into the North Atlantic by three major routes: (1) directly into the Irminger Sea, (2) into the eastern North Atlantic via the deep North Atlantic Current extension, and (3) equatorward as part of the Deep Western Boundary Current (DWBC). These routes are clearly seen in the lateral map of mid-depth PV from Talley and McCartney (1982), reproduced here as Fig. 1. The impression one gets from Fig. 1 is that all of the LSW emanates from the Labrador Sea.

Using the WOCE hydrographic data set of the 1990s, some of the recent transit-time estimates for LSW to spread into the open North Atlantic are surprisingly fast (e.g. Sy et al., 1997; Koltermann, 1999, see Fig. 1). Of particular note is the short communication time between the Labrador Sea and Irminger Sea, which is thought to be on the order of 6 months. Sy et al. (1997) based this estimate on the similarity in the time-varying

density of LSW observed in the two seas, as well as on the CFC concentrations, and they explicitly discounted the notion that LSW might be formed locally in the Irminger Sea.

### 2.2. Discrepancies in the rapid spreading view

It is important to realize that these fast transit times were derived without the use of wintertime data (none were available). Because of the quick restratification that can occur after deep convection (e.g. order weeks, see Lilly et al., 1999), this can mask the signature of local overturning and lead to misinterpretation. We believe this was the case for the (non-winter) Irminger Sea data used in the above studies.

#### 2.2.1. Early spring Irminger sections

In April 1991, two hydrographic sections were occupied southeast of Cape Farewell (see Fig. 4a for the locations of the sections). While not wintertime, this is much earlier in the year than any of the WOCE sections used by Sy et al. (1997). These sections were also done during the time of high NAO of the early 1990s (Fig. 2). The vertical profiles from the cruises show a pronounced, nearly uniform layer of LSW. For example, consider the R/V *Endeavor* section (see Table 1). At the offshore edge of this section the LSW layer extends to 1800 m, with a “re-stratifying” layer roughly 200 m thick at the top and bottom of the profile (seen in the potential density, Fig. 3a, and potential vorticity, Fig. 3b). Such a profile, which is representative of the sections, is indicative of a convectively overturned water column that has only recently begun to re-stratify. To demonstrate this, we compare the Irminger profile to a conductivity/temperature/depth (CTD) station from the Labrador Sea occupied in winter 1997<sup>2</sup> during the Deep Convection Experiment (Labsea Group, 1998; Pickart et al., 2002a). The water column was actively convecting at this time, and the profile shown was occupied during March within the region of deepest overturning in the western part of the basin (see Fig. 4a). One sees

<sup>2</sup>Winter in this context means December 1996–March 1997. This convention is used throughout the paper.

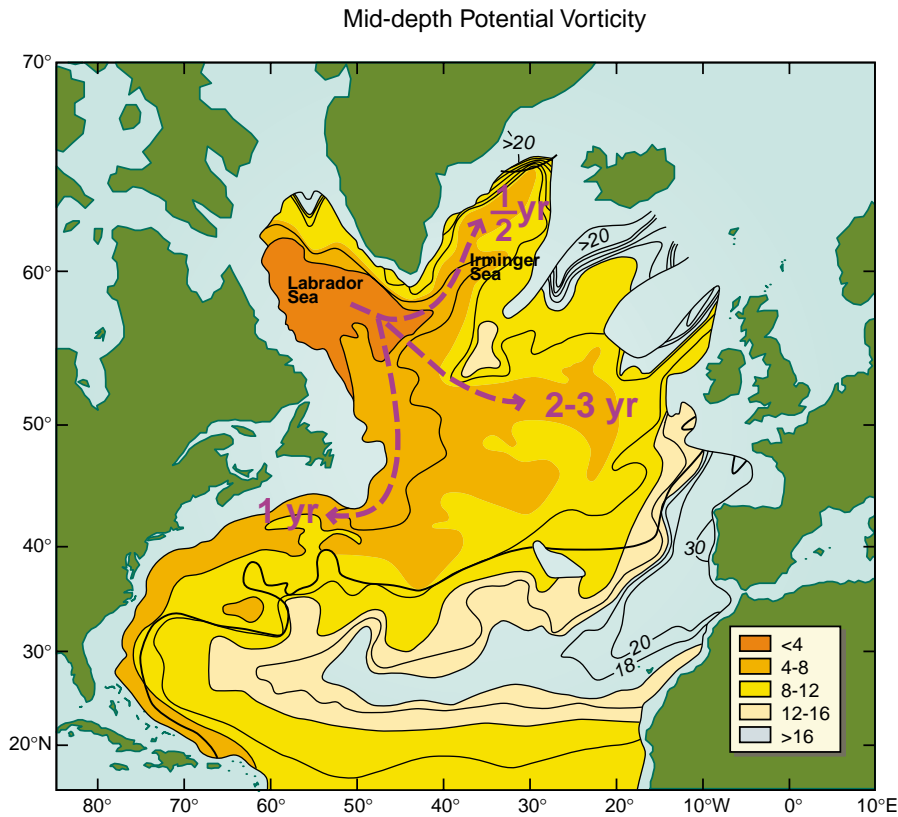


Fig. 1. Lateral distribution of mid-depth planetary potential vorticity ( $1/(\text{cms}) \times 10^{-14}$ ), adopted from Talley and McCartney (1982). Dashed lines denote the three principle spreading routes of LSW. The estimated transit times for each route are from Sy et al. (1997).

that convection had reached a depth of 1400 m, with a hint of restratification at the top and bottom (blue profiles in Figs. 3a and b).

Note the similarity in the potential vorticity profiles of the two stations, in particular that the PV is nearly zero (aside from small scale noise) over the majority of the LSW layer. Although the Irminger profile is clearly farther along in the restratification process, the Labrador profile—which was likely ventilated only days before the measurement was taken—shows the beginning of a surface buoyant cap over the top 200 m (the same range as the Irminger profile cap). The third station shown in Figs. 3a and b (green profiles) was taken in the southwestern Irminger Sea in fall 1991, roughly 5 months after the April profile (see Fig. 4a). Restratification, which is likely due to lateral eddy flux from the neighboring boundary

current system (Lilly et al., 1999), has influenced most of the layer at that point.

Our interpretation of Figs. 3a and b is that it shows three different stages of a convectively overturned water column: hours to days after convection (March Labrador profile), days to weeks after convection (April Irminger profile), and months after convection (September Irminger profile). We note that time series of buoyancy at the Ocean Weather Station BRAVO site indicate that convection can occur as late as April in the Labrador Sea (J. Lazier, personal communication). Further indication that the April Irminger profile was locally ventilated is given by the oxygen saturation (Fig. 3c). Clarke and Coote (1988) observed values of percent saturation in the range 93–94% during active convection in the Labrador Sea in winter 1976. This was

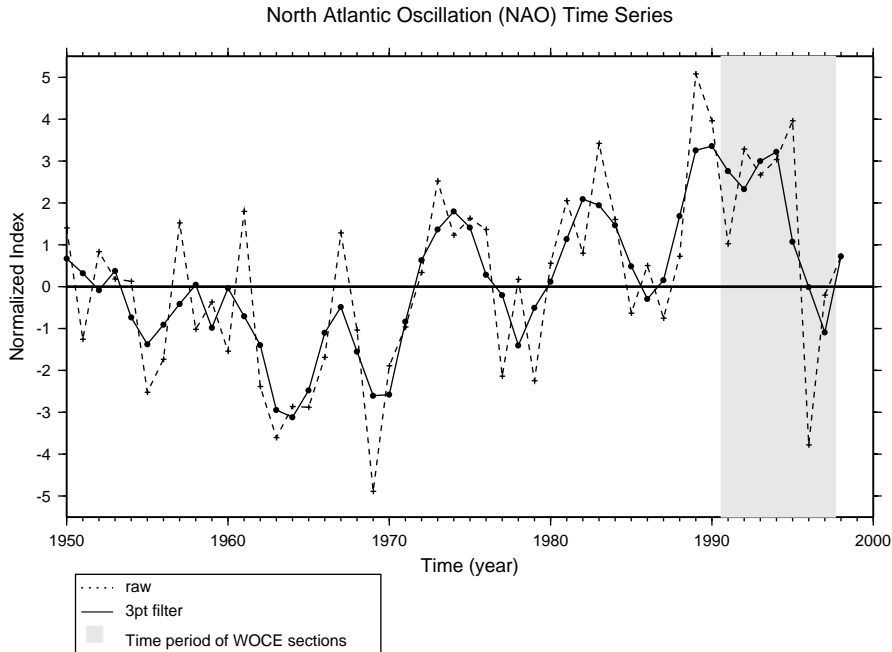


Fig. 2. Time series of the North Atlantic Oscillation wintertime index since 1950 (see text for definition of the index). Both the yearly values (dashed line) and 3-point running mean (solid line) are displayed. The time period of the hydrographic sections analyzed in the paper is indicated by the gray shading.

observed as well during the 1997 Deep Convection Experiment (Pickart et al., 2002a). The April Irminger profile shows values around 94% (slightly larger, in fact, than in the Labrador Sea in winter 1997).

We note that even if the April profile in Fig. 3 had not been ventilated locally in the Irminger Sea, the water was clearly formed somewhere during the winter of 1991. If we discount the evidence noted above and assume it was formed in the Labrador Sea, we can derive a travel time estimate as follows. We take the net distance to be that from the area of formation in the Labrador Sea (see Pickart et al., 2002a and Fig. 9) to the location of the R/V *Tyro* section in the Irminger Sea showing newly ventilated water on 20 April 1991. If we assume formation occurred at the beginning of February (which is probably early, see Lilly et al., 1999), this gives an elapsed time of 2.5 months and a transit speed of 13 cm/s. This is as strong as the (westward) DWBC at mid-depth. Such a strong flow is highly unlikely for an interior pathway in this part of the North Atlantic

(Lavender et al., 2000; Straneo et al., in press; see also Section 4).

#### 2.2.2. Property time series in the Irminger and Labrador Seas

To investigate further the connection between the LSW recently measured in the Irminger and Labrador seas, we systematically considered hydrographic sections occupied in the two seas during the time period 1990–1997 (Fig. 4). In the Labrador Sea all of the sections are occupations of the WOCE AR7W line (Lazier et al., 2002), which were occupied mostly in late spring (Fig. 4b). In the Irminger Sea some of the sections are the western portion of the WOCE A1E line (near 59–60°N), and others are independent surveys. Note that the Irminger Sea data have a much wider seasonal range, spanning spring, summer, and fall. Table 1 summarizes the cruises.

To facilitate a quantitative comparison, each of the sections was standardized as follows. First, the stations for each cruise were projected onto a common line for the specified basin (see Fig. 4a).

Table 1  
WOCE-Period hydrographic sections used in the study

Date	Cruise ID	Principal investigator
<i>Irminger Sea sections</i>		
20–21 Apr 1991	ENDEAVOR 223	Robert Pickart
20–22 Apr 1991	TYRO 91-1	Hendrik van Aken
19–22 May 1991	HUDSON 91007	Ross Hendry
19–20 Aug 1991	CHARLES DARWIN 9108	John Gould
05–07 Sep 1991	METEOR 18	Jens Meincke
15–19 Sep 1992	VALDIVIA 129	Alexander Sy
25–29 Nov 1994	METEOR 30/3	Jens Meincke
09–12 Jun 1995	VALDIVIA 152	Manfred Bersch
23–24 Jul 1996	VALDIVIA 16-I	Fritz Schott
12–13 Nov 1996	KNORR 147-IV	Mike McCartney
18–20 Jun 1997	KNORR 151-II	Lynne Talley
06–08 Aug 1997	DISCOVERY 230	Sheldon Bacon
<i>Labrador Sea sections</i>		
02–09 Jul 1990	DAWSON 90012	John Lazier
23–31 May 1991	HUDSON 91007	Ross Hendry
06–08 Jun 1992	HUDSON 92014	John Lazier
18–29 Jun 1993	HUDSON 93019	John Lazier
25 May–05 Jun 1994	HUDSON 94008	John Lazier
18–24 Nov 1994	METEOR 30/3	Jens Meincke
11–16 Jun 1995	HUDSON 95011	John Lazier
19–24 May 1996	HUDSON 96006	John Lazier
21–28 Oct 1996	HUDSON 96026	Allyn Clarke
27 Feb–06 Mar 1997	KNORR 147-V	Robert Pickart
21–27 May 1997	HUDSON 97009	Allyn Clarke

In the Labrador Sea this was trivial; in the Irminger Sea the projection (denoted as  $\sim A1E$ ) is roughly along the isobaths, which is sensible especially for the continental slope region. After the projection, the data were interpolated onto a common uniform grid using a Laplacian-spline interpolator (see Pickart and Smethie (1998) for details of this procedure). The properties considered were potential temperature ( $\theta$ ), salinity (salinities were calculated using the practical salinity scale and hence have no units), potential density referenced to the sea surface ( $\sigma_\theta$ ), and planetary potential vorticity (PV, in units of  $1/(\text{ms}) \times 10^{-12}$ ).

To construct a time series of LSW properties in each basin it is first necessary to define the LSW. We used the distribution of PV to do this, since PV is a particularly effective tracer of this water mass (see Talley and McCartney, 1982; Pickart et al., 2002a). This was done as a multi-step process.

First, vertical sections of PV were constructed for each cruise, and the broad body of LSW was identified using the  $PV = 4$  contour as the delimiter (Fig. 5). For example, in the August 1991 Irminger Sea section, the LSW is clearly confined to the layer between 500 and 1500 m, not the deep layer adjacent to the Reykjanes Ridge (which is the other region of low PV in the section). Next, the minimum value of PV was found within the broad lens of LSW for each section—this value had to account for at least 3% of the data points within the lens, thereby avoiding spurious data values. Finally, the LSW “core” was defined as the area  $\leq e^{0.75}$  of the minimum value for the Irminger sections, and  $\leq e^{1.5}$  for the Labrador sections.<sup>3</sup> In this manner we were able

<sup>3</sup>The values of the exponents were chosen so that the core areas were roughly the same in the two seas and confined fairly close to the PV minimum.

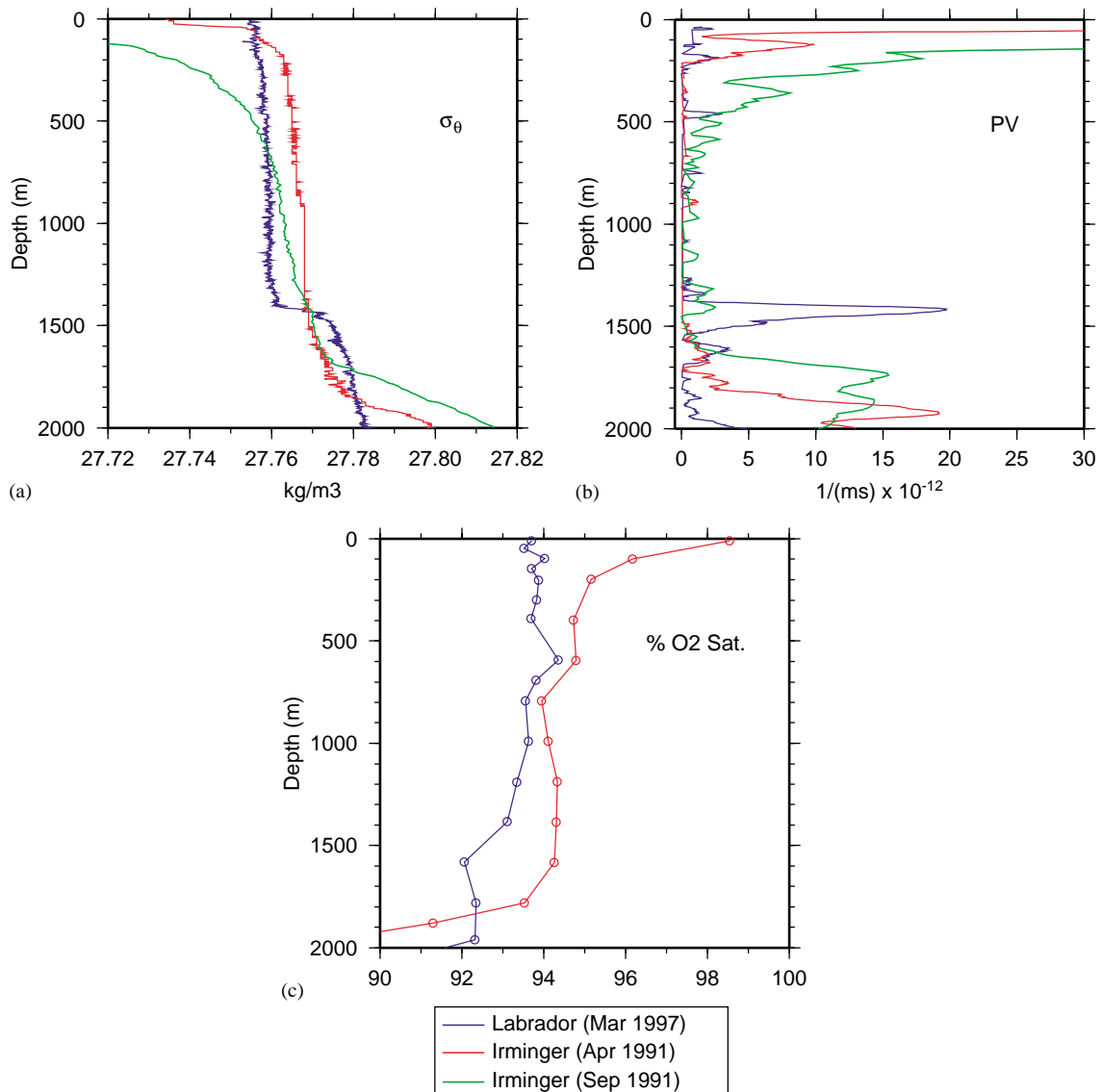


Fig. 3. Vertical profiles of (a) potential density, (b) potential vorticity, and (c) percent oxygen saturation, from the cruises indicated in the legend (the April 1991 Irminger profiles are from the R/V *Endeavor* cruise). See Fig. 4 for the locations of the stations.

to determine objectively the area of strongest LSW signature in each section. The value of LSW  $\theta$ ,  $S$ , and  $\sigma_\theta$  for each cruise is the average value computed over the core region. (Defining the core simply by the  $PV = 4$  contour leads to similar results.)

The time series of LSW properties for the two basins are shown in Fig. 6. In general, a warmer

and saltier type of LSW is found in the Irminger Sea (Figs. 6a and b), which Sy et al. (1997) argued is due to mixing as the water spreads north-eastward from the Labrador Basin. Their argument for rapid spreading is based on the similarity in density of the LSW observed in each basin (Fig. 6c), in particular the increase in  $\sigma_\theta$  from the early 1990s to 1995. However, consideration of the

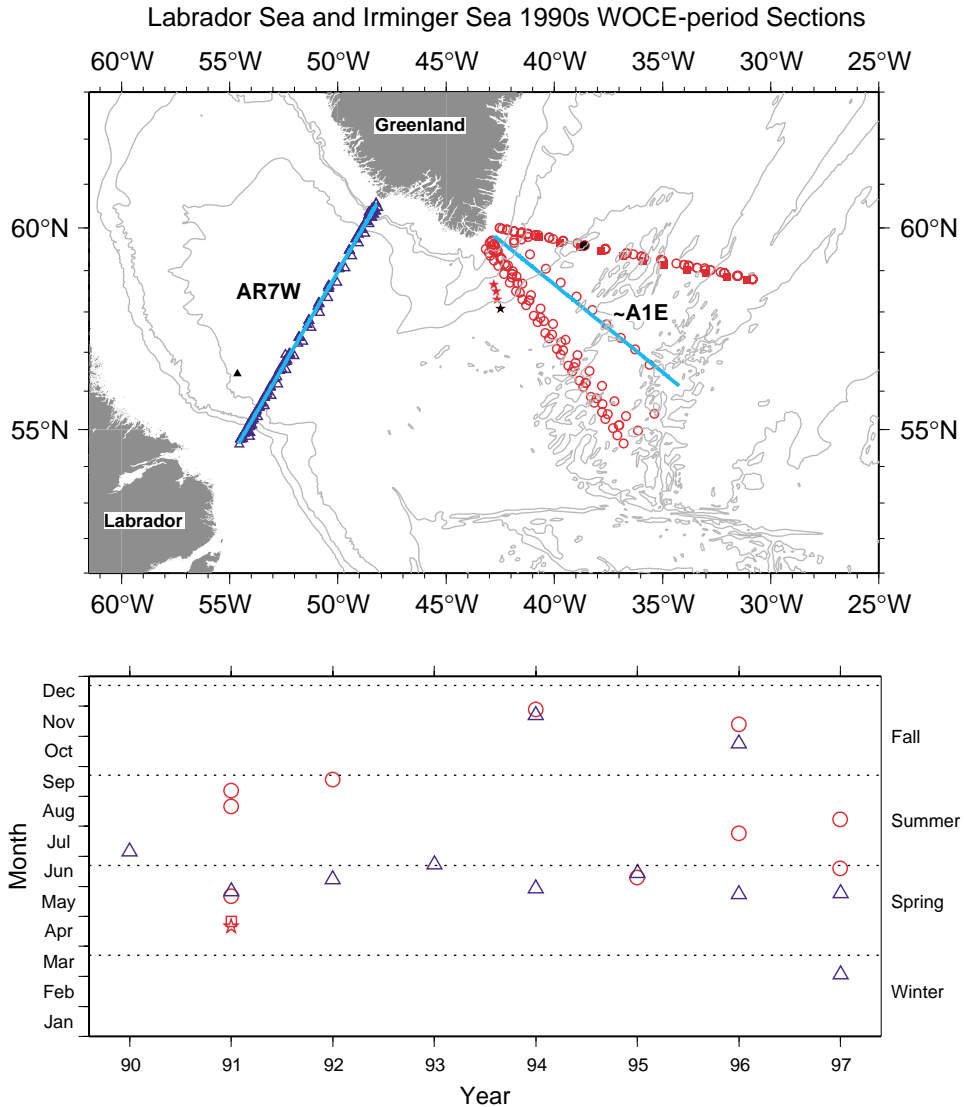


Fig. 4. Hydrographic data used in the study. Labrador stations are blue, Irminger stations are red. This color convention is used throughout the paper. (a) Locations of the sections, and the two regression lines (which are referred to as AR7W and ~A1E, in cyan). The two April Irminger Sea sections discussed in the text are denoted by stars (R/V *Endeavor* cruise) and squares (R/V *Tyrol* cruise). The individual profiles displayed in Fig. 3 are colored black. The isobaths shown are 1000, 2000, and 3000 m. (b) Temporal distribution of the sections.

longer  $\theta$  and S time series in Figs. 6a and b casts doubt on such a simple scenario. A rapid advective link between the two basins should mean that all the LSW properties track each other closely (with perhaps a short lag). This is not the case. For instance, the salinity history of the two basins is

markedly different: the LSW in the Labrador Basin became progressively saltier in the latter half of the 1990s, while the Irminger Sea LSW became slightly fresher over this time period (Fig. 6b). Dickson et al. (2002) have documented that the Denmark Strait overflow water has become fresher

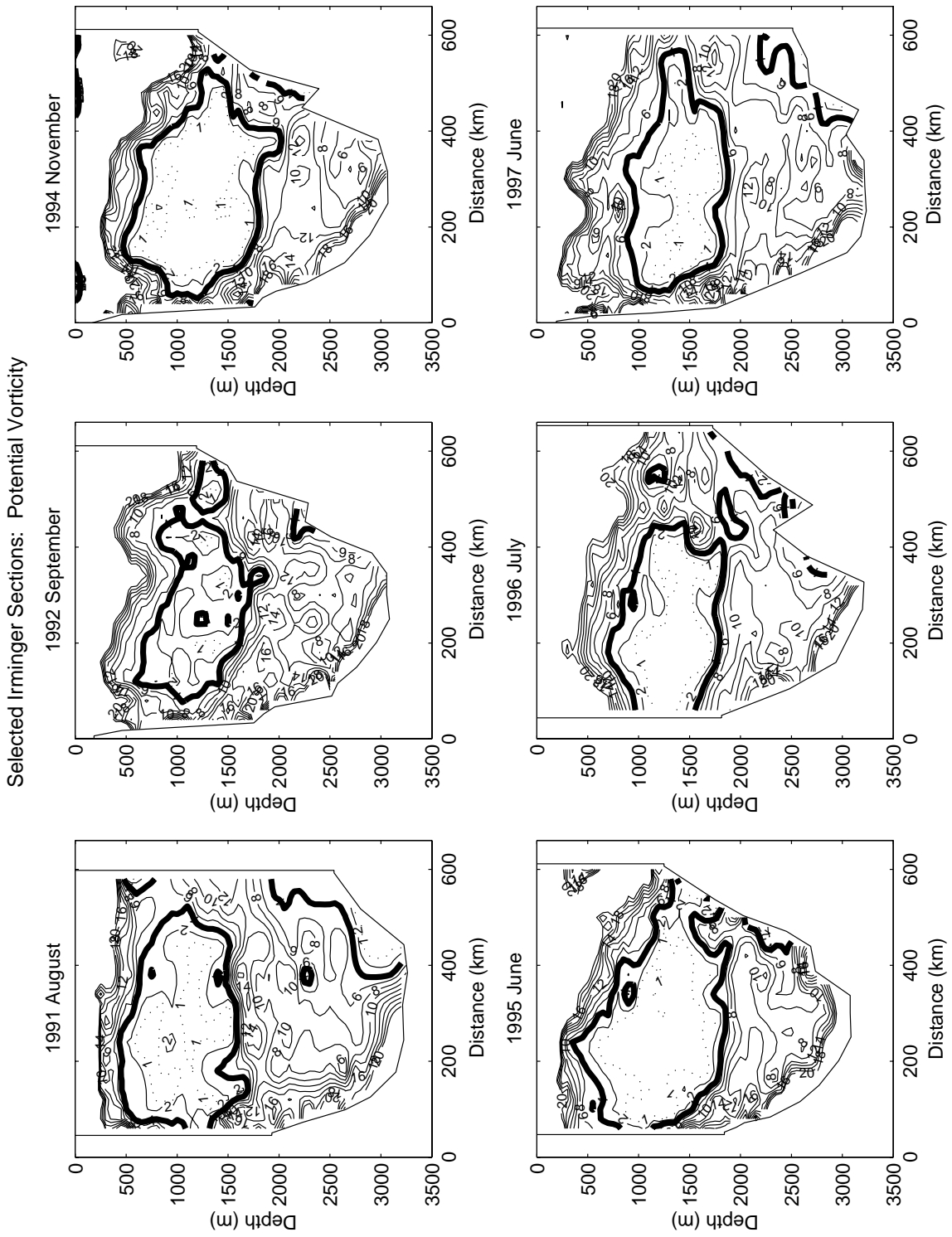


Fig. 5. Vertical sections of potential vorticity (PV) in the Irminger Sea, after standardization onto the uniform grid as described in the text. The bold contour is  $PV = 4$ .

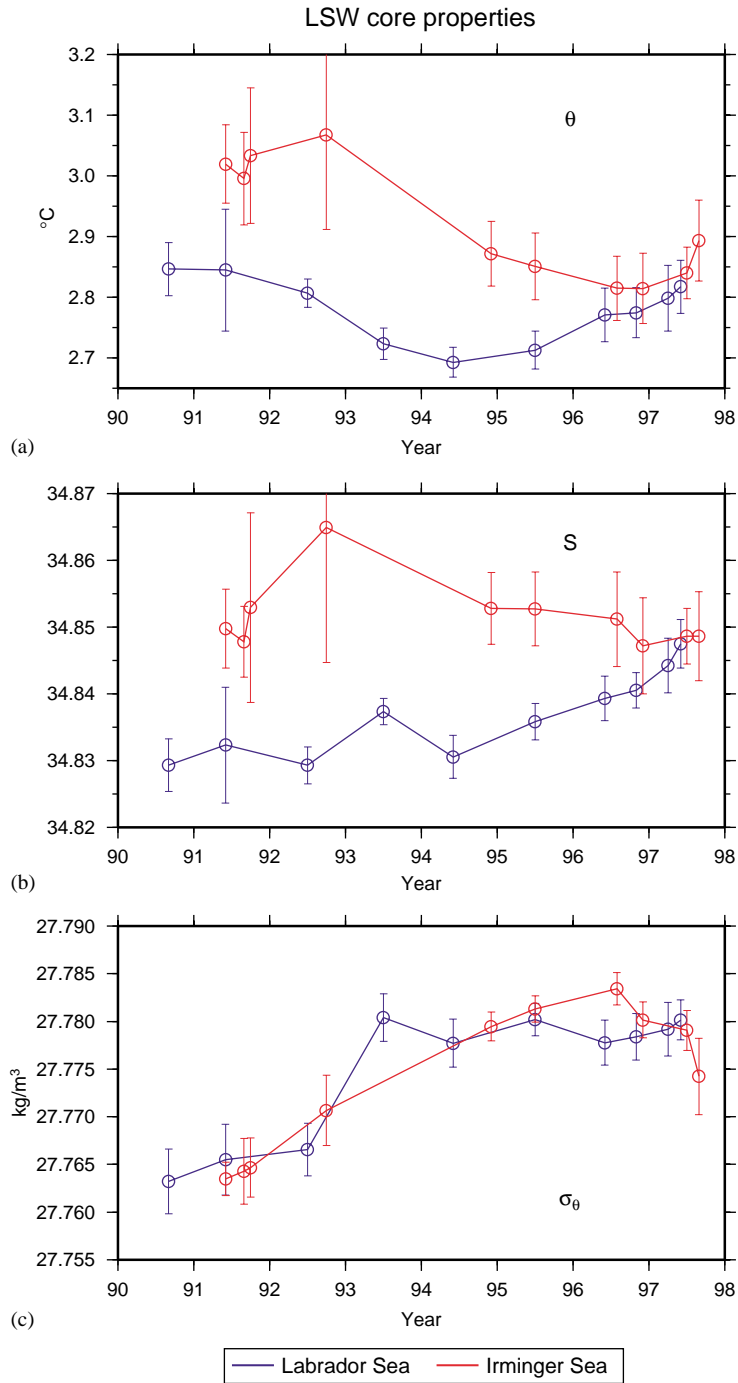


Fig. 6. Time series of the LSW core properties in each basin. The standard deviation is indicated by the bars. (a) Potential temperature, (b) Salinity, (c) Potential density.

during this time period as well, so one might wonder if the Irminger Sea LSW signal is influenced by mixing with the overflow water. This is unlikely, since the overflow water sinks to a deeper depth immediately southward of the sill, well upstream (and onshore) of the pool of low PV Irminger Sea LSW.

In the next section we argue that local formation of LSW is likely occurring in the Irminger Sea. We believe, however, that *slow* spreading from the Labrador Sea plays a significant role as well. This is discussed further in Section 4.2, where we return to the time series of Fig. 6.

### 3. Evidence for Labrador Sea Water formation in the Irminger Sea

#### 3.1. Historical measurements

The idea that deep convection takes place in the Irminger Sea is not new by any means. As early as the beginning of the 20th century oceanographers suspected that deep (or bottom) water formation occurred southeast of Greenland (Nansen, 1912). In fact, this location was identified before the Labrador Sea. However, the early evidence for sinking in the Irminger Sea was circumstantial to say the least, so the idea remained more of a hypothesis for quite some time. It was not until the 1930s that the first wintertime data were collected in the Irminger Sea, during two expeditions of the R/V *Meteor* (Defant, 1936). Part of the motivation for this field program was in fact to verify Nansen's earlier hypothesis. The hydrographic stations from the *Meteor* surveys revealed a ventilated, weakly stratified water mass in the southwest Irminger Sea (Wattenberg, 1938; Wust, 1943)—undoubtedly what today we would call newly formed LSW. Non-winter data from this region, collected during the extended high-NAO period from 1903 to 1915, also show deep-reaching LSW (with a buoyant cap), consistent with the 1991 Irminger profiles discussed above (Nielsen, 1928).

Oddly, this “proof” of convection in the Irminger Sea did not influence the oceanographic community enough to establish the Irminger basin as a major site for the formation of LSW. Instead,

the Labrador Sea garnered most of the attention, and through the years the notion of deep overturning east of Greenland has become all but forgotten. There are likely several reasons for this. For example, measurements collected at Ocean Weather Station BRAVO in the Labrador Sea showed evidence of local convection (Lazier, 1980), whereas data from Ocean Weather Station ALPHA in the Irminger Sea did not. This is due to the fact that BRAVO was situated near the region most predisposed for overturning to occur in the Labrador basin (Pickart et al., 2002a), but ALPHA is so far offshore of the Greenland landmass that the air–sea forcing is insufficient to drive convection there (see Fig. 13). This is discussed further below.

As of late, much effort has been spent studying convection in the Labrador Sea (see for example the special issue on convection in the January 2002 issue of *Journal of Physical Oceanography*), further emphasizing the Labrador Sea as the sole origin of LSW. It must be remembered, however, that there are data that show “mode water” in the Irminger Sea as deep, and as weakly stratified, as that in the Labrador Sea. Furthermore, the lateral display of PV in Fig. 1, implying a Labrador Sea–only source, uses data from a time period during which the NAO was moderate to low. In Section 4.1 we use climatological data to present a different view of the lateral distribution of LSW, which is suggestive of an Irminger Sea source as well.

#### 3.2. Conditions for convection

In order for deep convection to occur in the open ocean, a fairly well-defined set of conditions needs to be satisfied. Roughly speaking, these are (1) sufficient oceanographic preconditioning (i.e. weakly stratified ambient water), (2) closed cyclonic circulation (trapping of water), and (3) strong air–sea buoyancy fluxes (wintertime densification of the surface water). This “equation for convection” is satisfied at the different convective sites of the North Atlantic (see Marshall and Schott, 1999): the Greenland Sea, the Mediterranean Sea, and the Labrador Sea. We argue now that it is satisfied in the Irminger Sea as well.

### 3.2.1. Oceanographic preconditioning

Deep convection is facilitated when weakly stratified, dense water resides near the sea surface (e.g. MEDOC group, 1970). This is evident in the Labrador Sea, for example, where mid-depth isopycnals dome upward towards the center of the basin (e.g. Lazier and Wright, 1993). We used the collection of recent hydrographic sections described above to investigate this. The mean sections of  $\sigma_\theta$  (Fig. 7) show a doming of isopycnals in both basins (the lateral extent of the dome is smaller in the Irminger Sea). One might suspect, however, that the ambient water in the Labrador Sea is more weakly stratified and hence more preconditioned. To see if this is true we constructed mean vertical profiles of  $\sigma_\theta$ , where the mean is restricted to the area of the dome, using data only from late spring/early summer (in order to exclude seasonal effects). As expected, the layer of LSW in the Irminger dome is warmer and saltier than that in the Labrador Sea (Figs. 8a and b). However, the temperature and salinity completely compensate each other in the Irminger Sea, so that the profiles of density in the two basins are virtually indistinguishable to a depth of 1500 m (Fig. 8c). Since density—not temperature or salinity—determines to first order the extent of convective overturning, this demonstrates that the Labrador Sea is no more preconditioned than the Irminger Sea.<sup>4</sup>

### 3.2.2. Regional circulation

As discussed in Clarke and Gascard (1983), an important aspect of deep convection is the trapping of water within a closed gyre in the region of the wintertime atmospheric forcing. This keeps the surface water from being advected away from the area, thereby subjecting it to the buoyancy loss for a longer period of time. Recently, Lavender et al. (2000) constructed a mean description of the mid-depth circulation in the western subpolar North Atlantic using a composite of Profiling Autonomous Lagrangian Circulation Explorer (PALACE) float data. Their map of absolute

pressure anomaly at 700 m is reproduced as Fig. 9, which shows a series of closed, sub-basin scale cyclonic recirculations, extending from the Irminger basin to the Newfoundland basin. These gyres were previously undetected because of their largely barotropic nature (hence they are not evident in geostrophic shear measured from hydrography). The float data indicate that the gyres are present year-round (Lavender, 2001). Spall and Pickart (2002) argue that they are driven by the local windstress curl in the vicinity of Greenland.

Based on the above argument regarding trapping of water, one might expect to observe the deepest overturning within these gyres. This indeed seems to be the case in the Labrador Sea. In the winter of 1997 the deepest mixed-layers were observed in the trough of the western recirculation (Fig. 9). As discussed by Pickart et al. (2002a), convection did not occur farther north in this gyre because of the lack of preconditioning there. In winter 1978 the densest water was also formed in precisely this same area (Clarke and Gascard, 1983), adding further credence to the notion that the circulation plays an important role. We are unable to make the analogous plot of mixed-layer depth for the Irminger Sea, since there were no wintertime hydrographic surveys during the 1990s. In fact, there have been no basin-wide wintertime surveys in the Irminger Sea ever during high-NAO conditions. However, we did the next best thing using our mean Irminger PV section. Specifically, we calculated the PV across the section at the depth of the LSW core, which is shown in relation to the observed circulation in Fig. 9. One sees that the lowest PV water is found in the trough of the Irminger gyre. Thus, in both seas, the water of strongest convective origin is “trapped” within a local recirculation.

### 3.2.3. Atmospheric forcing

The final requirement for deep convection to occur in an ocean basin is strong atmospheric buoyancy forcing. In the Labrador Sea this is associated with the dry, polar air that blows off of the Canadian land mass over the relatively warm surface water during winter. More specifically, the southern Labrador Sea lies along the North

<sup>4</sup>The effect on overturning due to the dependence of the thermal expansion coefficient on temperature is minimal, as was documented using the mixed-layer model of Section 3.2.3.

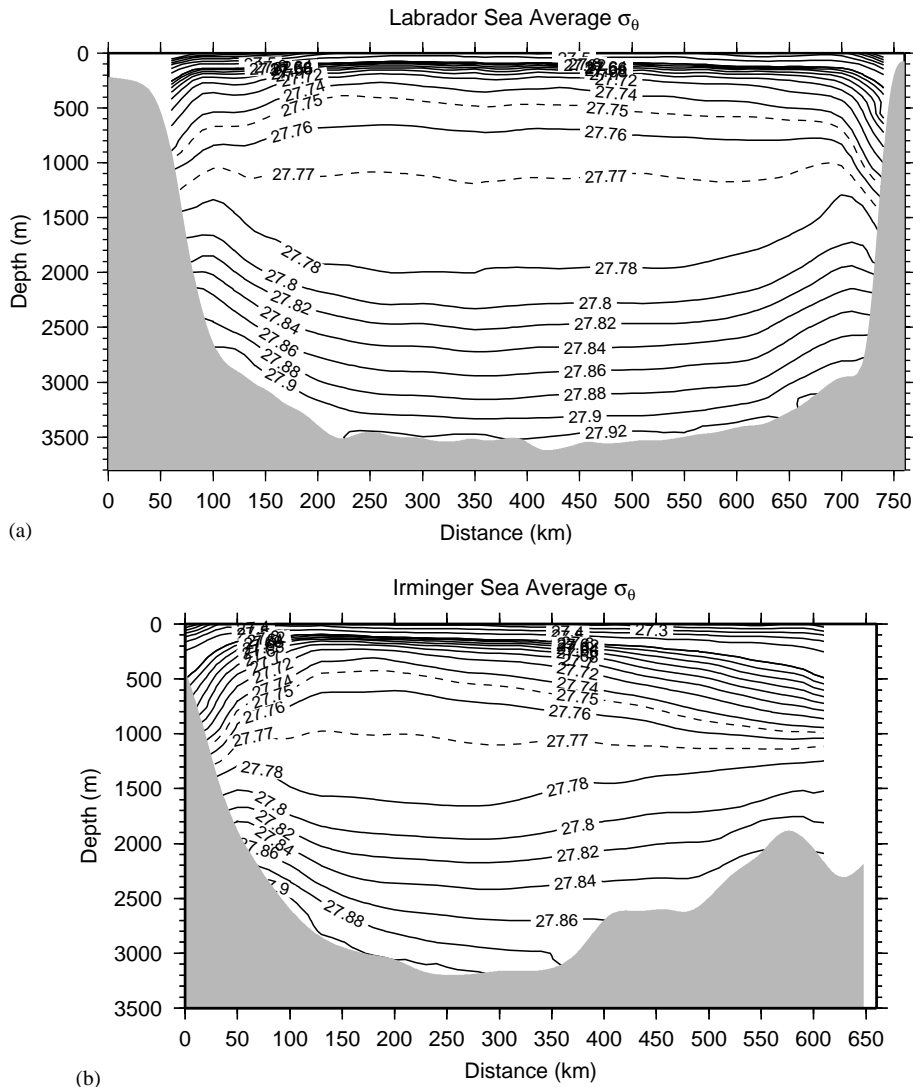


Fig. 7. Average sections of potential density for the time period 1990–1997 (see text for explanation). (a) The Labrador Sea. (b) The Irminger Sea.

Atlantic winter storm track (this tends to be more true during high-NAO winters, when the storm track is shifted northwards, Dickson et al., 1996), and the cyclonic flow associated with low-pressure systems transiting the area causes large heat flux events over the basin (Renfrew et al., 1999; Pagowski and Moore, 2001). It is the cumulative effect of these storms that causes the formation of LSW.

During the 1997 field experiment studying convection in the Labrador Sea, extensive air–sea flux measurements were made during the winter season (Labsea Group, 1998; Bumke et al., 2002; Renfrew et al., 2002). Using these data as ground truth, Renfrew et al. (2002) investigated the ability of the National Centers for Environmental Prediction (NCEP) reanalysis to capture the wintertime variability in the surface meteorological and

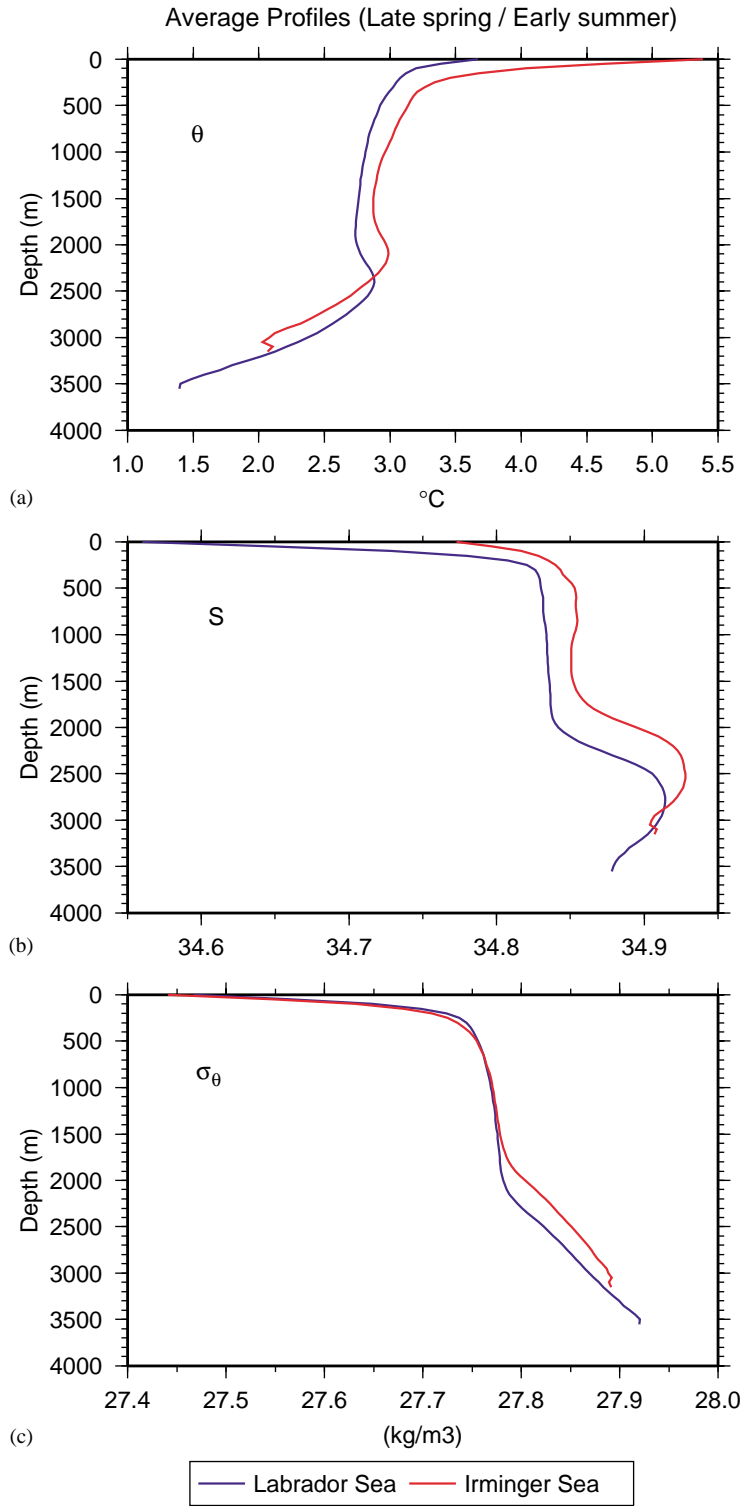


Fig. 8. Mean vertical profiles of (a) Potential temperature, (b) Salinity, (c) Potential density, averaged over the region of the isopycnal dome, for the late spring/early summer time period.

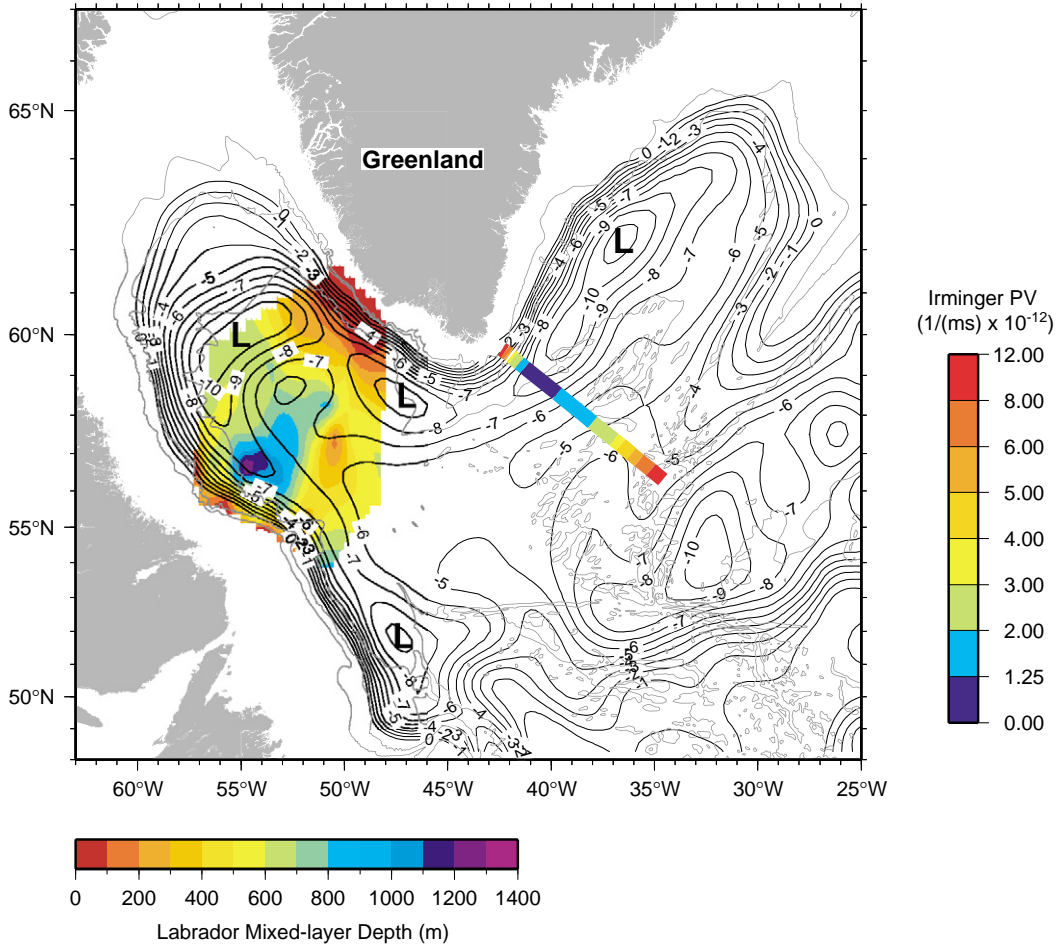


Fig. 9. Absolute pressure anomaly at 700 m (contour lines) from Lavender et al. (2000), revealing the series of sub-basin scale recirculations in the western sub-polar gyre (these are denoted by “L”, indicating low pressure). Overlaid is the distribution of Labrador Sea mixed-layer depth in winter 1996–1997, from Pickart et al. (2002a), and the average mid-depth potential vorticity along the ~A1E line in the Iringer Sea (see text for details). The isobaths are 1000, 2000, and 3000 m.

air–sea flux fields over the Labrador Sea. They showed that the meteorological fields compared well with the observations but that the model heat fluxes had a systematic bias towards higher values. It was argued that this bias is the result of roughness length formulations for heat and moisture in the NCEP reanalysis that are inappropriate in conditions of high winds. They further showed that the bias is greatest (approximately 50%) during events characterized by large air–sea temperature differences. Better agreement with the direct turbulent measurements made by Bumke

et al. (2002) was obtained when a bulk flux formulation following Smith (1988), with the transfer coefficients of DeCosmo et al. (1996), was applied to the surface fields from the reanalysis. Subsequently, Moore and Renfrew (2002) produced ‘adjusted’ NCEP heat flux fields, which provide a more accurate description of the atmospheric forcing over the western subpolar North Atlantic. Here we use the adjusted fields for the 20 yr period from 1979 to 1998 to investigate the difference in air–sea forcing over the Labrador and Iringer Seas.

**3.2.3.1. High-NAO mean fields.** We first constructed the mean representation for a high-NAO winter, by averaging all winters (DJF) in which the NAO index was greater than one (see Fig. 2). This is appropriate, since it is under such conditions that convection occurs in the western subpolar North Atlantic (e.g. Dickson et al., 1996). The high-NAO mean winter fields show a strong minimum in sea-level pressure centered east of Cape Farewell (the Icelandic Low, Fig. 10a), with strong northwesterly winds over the Labrador Sea, and northerly winds east of Greenland in the Irminger Sea. In both locations the winds blow off the landmass (Labrador and Greenland) over the ocean, resulting in elevated heat loss in the western portions of each basin (Fig. 10b). The mean winter heat flux in the Labrador Sea is strongest in the northwestern part of the basin, and is greater than that in the Irminger Sea east of Cape Farewell. However, as noted above, the ambient water in the northern part of the Labrador Sea is not preconditioned for convection (see Pickart et al., 2002a). Thus, the atmospheric forcing over the region where convection actually occurs in the Labrador Sea is not terribly different than that in the western Irminger Sea (about 30% more, though the difference may be less, see below).

**3.2.3.2. Synoptic-scale events.** It is of interest to examine the impact of individual storms on the two basins. To do this we considered the 6-hourly NCEP reanalysis data for all Februaries during the 20 yr time period. Specifically, we computed the cross-correlation between the total turbulent heat flux at a site in the southern Labrador Sea and various surface meteorological fields over the surrounding subpolar North Atlantic. The procedure was then repeated for a site in the western Irminger Sea. This approach is more robust than simply constructing composites of strong heat flux events, since no selection criteria must be made. The cross-correlations are dominated by the synoptic variability, as the lagged correlations of the individual fields are typically small. The statistical significance of the cross-correlation fields was determined with the Student's *t*-test. The results indicate that synoptic-scale heat flux events in both seas are associated with coherent

and statistically significant atmospheric circulation patterns across the North Atlantic.

The computed cross-correlations are shown in Fig. 11. All quantities are normalized so that the maximum value does not exceed unity (for example an eastward-pointing vector with magnitude equal to one implies perfect correlation between the total heat flux and westerly wind). The physical interpretation of Fig. 11 is straightforward. In the Labrador Sea (Fig. 11a), a canonical high heat flux event is associated with a low-pressure system situated near Cape Farewell, characterized by increased westerly winds and colder surface air temperatures extending southwards from the Labrador Sea. In the Irminger Sea (Fig. 11b), the strongest heat flux events tend to occur when a low-pressure system is situated in the vicinity of Iceland, with colder air temperatures southeast of Greenland, and enhanced northwesterly winds off of the Greenland plateau. Hence, according to the NCEP climatology, there is a strong similarity in the pattern of the synoptic buoyancy forcing over both the Labrador and Irminger Seas.

It is important to note that the winds emanating from Greenland are not presently well represented in the NCEP data. The complex and steep topography of East Greenland exerts a strong influence on the surface wind field in this region (Heinemann, personal communication), and the coarse resolution of the global reanalysis calls into question the fidelity with which such winds are represented. For example, the NCEP model is unable to resolve a local jet that often develops in the lee of Cape Farewell, known as the Greenland Tip Jet (see Doyle and Shapiro, 1999). High-resolution atmospheric models indicate that this phenomenon results in elevated heat fluxes over the southwestern Irminger sea (Doyle and Shapiro, 1999; Pickart et al., 2002b).

This problem is exacerbated further when the formation of sea ice in the lee of East Greenland is considered. In general, ice is not very well handled in the global weather products, since both NCEP and the European Center for Medium Range Weather Forecasting (ECMWF) use a simple ice/no ice condition. Hence there is reason to suspect that the offshore extent of winter ice in the western

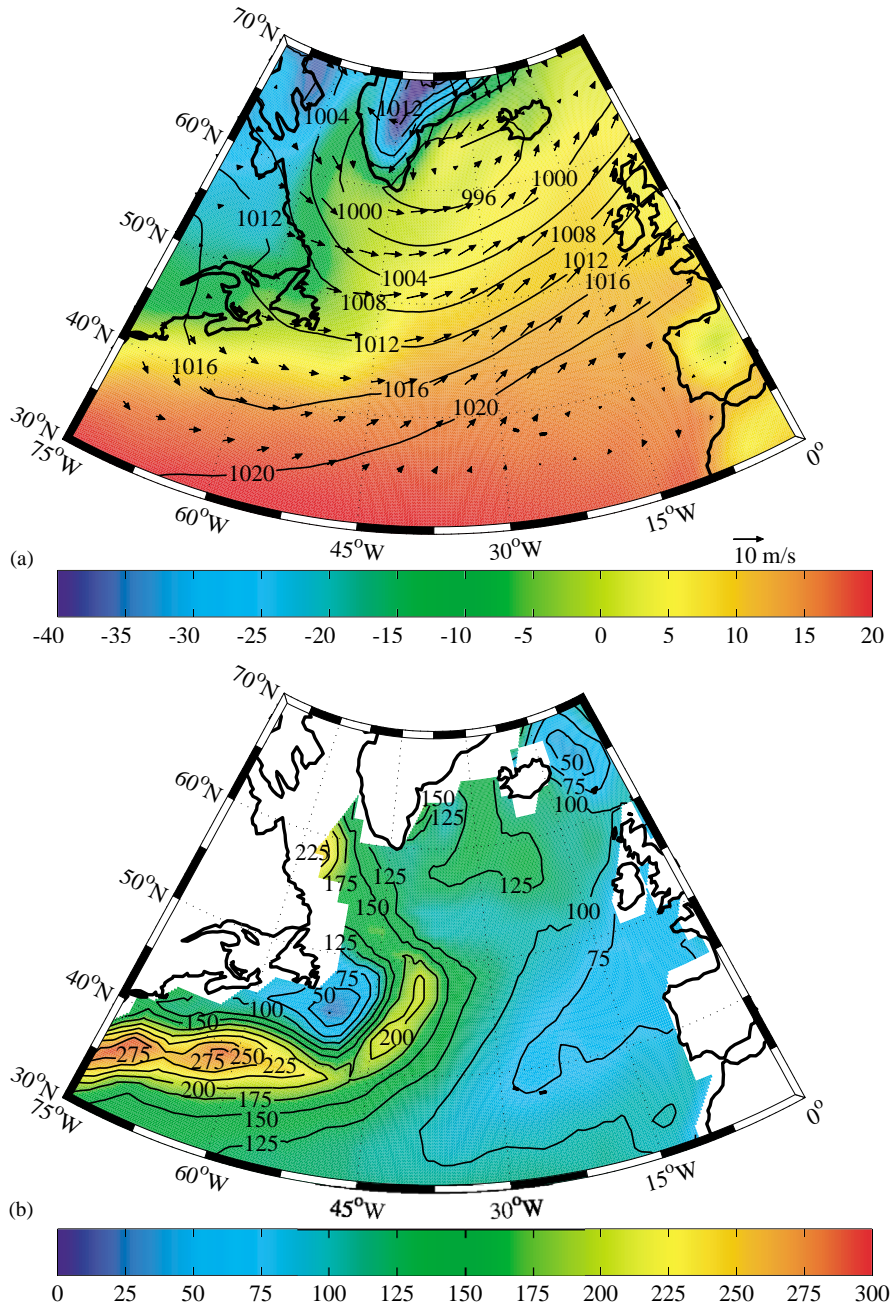


Fig. 10. Average winter fields for the high-NAO winters (see text for criterion) in the adjusted NCEP data set. (a) Sea-level pressure (contours in mb), 2 m air temperature (color in °C), and 10 m winds (vectors); (b) Total turbulent (sensible + latent) heat flux ( $\text{W}/\text{m}^2$ ), where positive values denote heat loss from the ocean.

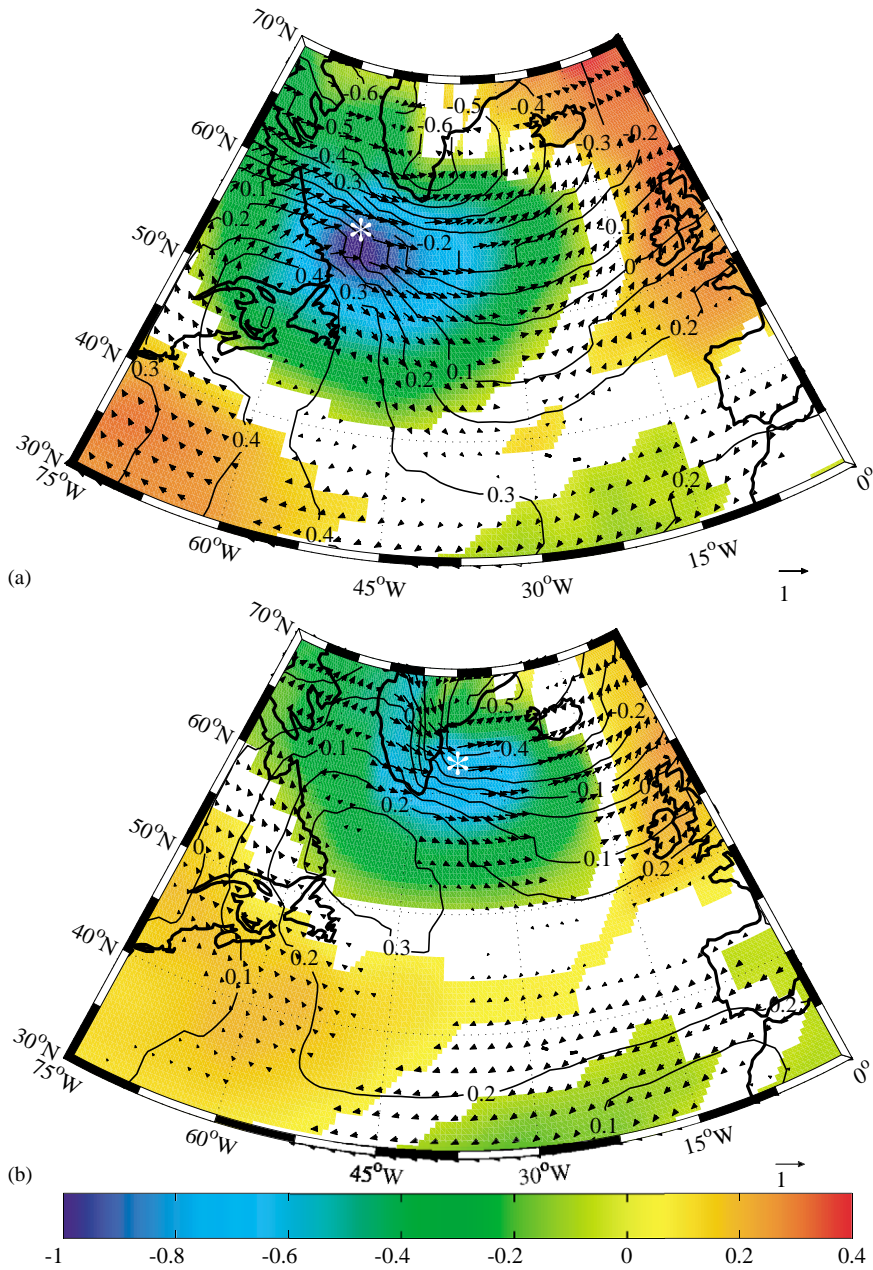


Fig. 11. (a) Cross-correlation between the total heat flux at a location in the Labrador Sea (indicated by the asterisk) and the sea-level pressure (contours), 2 m air temperature (color), and 10 m winds (vectors). Only regions of significant correlation at the 95% level are shown (see text for details). (b) Same as (a), except for a location in the Irminger Sea (denoted by the asterisk).

Irminger Sea is underestimated. Anecdotal support for this comes from the fact that the R/V *Tyro* encountered the ice edge near the 2000 m isobath

as it occupied the WOCE A1E line in April 1991 (van Aken, personal communication). This is substantially farther offshore than suggested by

the satellite data (from the National Snow and Ice Data Center) for that month. This type of error is potentially significant because the presence of sea ice would shift the heat loss maximum farther offshore (since there is essentially no heat loss over the ice). This in turn would mean greater buoyancy forcing over the portion of the Irminger Sea well preconditioned for convection. This points to the need for high-resolution atmospheric modeling to sort out such issues—a topic for future study. For the present purposes, the reader should keep in mind that the Irminger Sea heat flux in the lee of Greenland—even the adjusted NCEP product used here—is likely underestimated.

**3.2.3.3. Mixed-layer model.** It is of course the integrated effect over the winter that governs the extent of convection and the water mass transformation. Ignoring any of the potential errors in the heat flux noted above, we applied the NCEP forcing in a simple one-dimensional mixed-layer model to investigate the convective products in the two seas. The model is the same as that used by Clarke and Gascard (1983) and Pickart et al. (1997) to study water mass characteristics in the Labrador Sea. (The same evaporation rate was applied as in the earlier studies, though this has little bearing on the results below.) First, we applied the model to the two density profiles of Fig. 8c, since these represent the mean conditions in the two seas over the 8 yr period of interest. The average high-NAO winter forcing (total heat flux) for the 20 yr NCEP data set over the appropriate region in the Labrador Sea is  $235 \text{ W/m}^2$ , and for the Irminger Sea it is  $165 \text{ W/m}^2$ . The evolution of the mixed-layer in the two regions, over the 4 month winter period, is shown in Fig. 12. For the Labrador profile, convection occurs to  $> 2000 \text{ m}$  in mid-February, which is not unreasonable for a high-NAO period. In the Irminger Sea the mixed-layer takes longer to deepen, reaching  $1500 \text{ m}$  by late March. The final density of the two products is within the LSW range (Pickart et al., 1997).

Ideally, of course, one should use a density profile from late fall rather than early summer. In Fig. 4 it is seen that there were two fall surveys in each sea in our collection of sections: 1994 and 1996. The former was a year of strong convection

(I. Yashayaev, personal communication), and the latter represents the opposite extreme in which the NAO was very low and convection was virtually absent. In Fig. 5 one sees the difference in the LSW of the Irminger basin in these two years, in particular the reduced volume and higher stratification in 1996. Unfortunately, the fall 1994 Labrador Sea cruise did not obtain data outside the boundary current because of inclement weather, so we can consider only the latter year for the Labrador Sea.

Applying the mixed-layer model to a representative fall 1994 Irminger profile (Fig. 12), one sees the effect of the seasonal stratification in that the mixed-layer stays shallower for a longer time (compared to the early summer profile used above). However, at the end of February the mixed layer abruptly deepens as the stratified upper layer is eroded, and convection reaches  $> 1800 \text{ m}$ . The reason for this rapid evolution is that the intermediate layer was well preconditioned from the preceding strong winter. The final density of the water in this case is even closer to the LSW formed in the Labrador Sea, plus the deep convection commenced earlier in the season, more in line with observations in the Labrador Sea. Hence, even though we are forcing the Irminger profile with a heat flux that is likely too small, the mixed-layer model predicts that deep convection can occur in the Irminger Sea. By contrast, when the fall 1996 profiles are used, convection is restricted to less than  $700 \text{ m}$  in both the Labrador and Irminger Seas (not shown). This is because the water column was less preconditioned after the weak winter of 1995–1996.

## 4. Tracer distributions in the Labrador and Irminger Seas

### 4.1. Observations

Talley and McCartney's (1982) lateral distribution of PV (Fig. 1) has come to be known as the canonical scenario of LSW formation and spreading, i.e., the Labrador Sea-centric viewpoint. It is based on data from 1954 to 1964, and was constructed using the “core method”, whereby

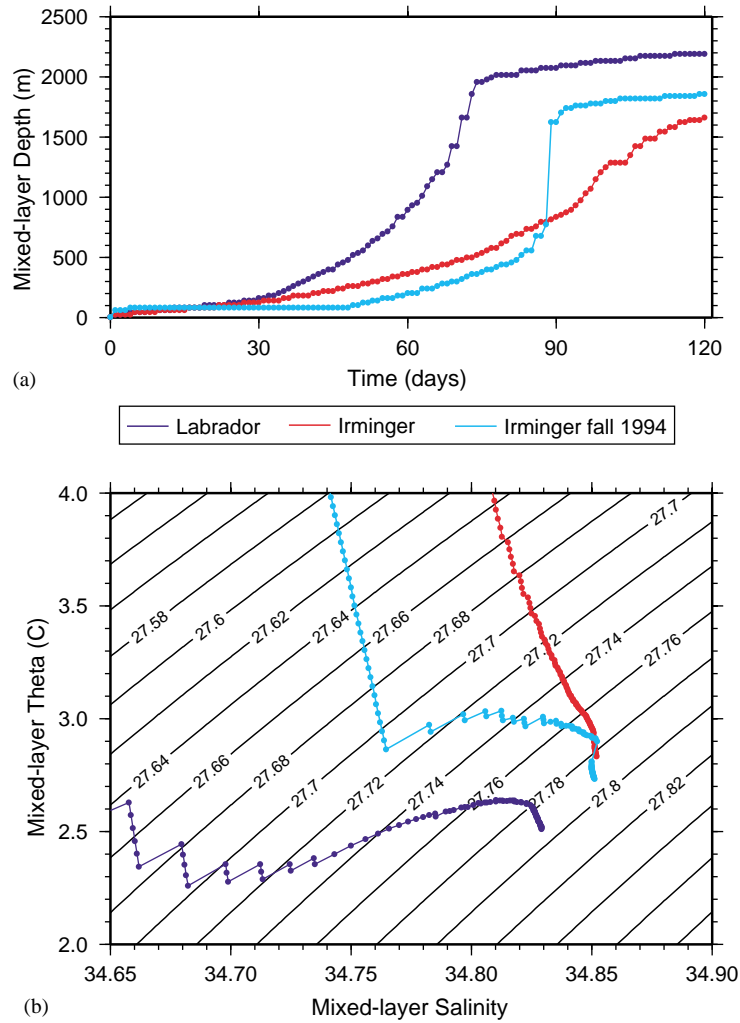


Fig. 12. Time series of properties from the mixed-layer model, using three different initial density profiles (see text). (a) Mixed-layer depth, (b) mixed-layer potential temperature and salinity (contours are potential density in  $\text{kg/m}^3$ ).

the mid-depth extremum in PV is identified from station to station. Using a more complete historical climatology, and also considering more recent data collected during the 1990s WOCE period, we now offer another view of the lateral PV field, one that gives a different impression with regard to the source of the low PV water.

The data used in the Talley and McCartney (1982) study come from a time period in which the NAO was moderate to low (Fig. 2). Based on the strong relationship between the NAO and convec-

tion in the western subpolar gyre (Dickson et al., 1996), as well as the discussion regarding the atmospheric forcing presented above, such a time period would be biased toward unfavorable convective conditions in the Irminger Sea. To investigate this we used HydroBase 2, a revised version of the Curry (1996) climatology of the North Atlantic. HydroBase 2 includes the World Ocean Database 1998, as well as data from the recent North Atlantic WOCE program and other individual experiments. The utilities within

HydroBase 2 allow the user to construct customized climatological mean fields (for example vertical and lateral sections), where the averaging is done on density surfaces. Such averaging has been shown to produce more accurate results than depth-averaged climatologies (see for example Curry, 2002).

We constructed various lateral maps of PV, emphasizing different time periods. For each map, the pressure, temperature, and salinity data were averaged (along isopycnals) into one degree bins. PV was then obtained using a running vertical window of 100 m, over which the vertical gradient of density was calculated. Gaps in the lateral sections were filled by Laplacian–Spline interpolation. We show results on depth surfaces, as there is no a priori reason to expect that convection in the Labrador and Irminger Seas should always produce water of the same density (even though this was the case for the recent WOCE period as noted above). We excluded the months of January to April in part of our analysis, since isolated wintertime measurements of PV (i.e. particularly low values near zero, see Fig. 3) can unduly influence the average. This was especially true for the recent WOCE period, where the 1997 February/March Labrador Sea data and 1991 April Irminger Sea data dominated the PV distributions. For longer time periods this was not a problem.

Consider first the WOCE time period 1989–1997. Fig. 13a shows the non-winter PV at 1000 m, which can be thought of as the analog to Fig. 1 for a high-NAO period. One sees that there are now two extrema of low PV, one in the Labrador Sea and one in the southwestern Irminger Sea. (Since the winter data have been excluded, this represents an adjusted state after convection subsides.) While there is low PV in the area between these two features, the Irminger Sea minimum is a robust and significant signal; it appears just as strongly when the map is made on the  $\sigma_\theta = 27.77$  density surface, which corresponds to the center of the LSW lens in each sea (Fig. 7). Adding further support is the fact that oxygen at this depth/density horizon contains an extremum of high concentration in each sea (not shown). A map of CFCs from data collected in 1997 (Rhein et al.'s (2002), Figure 8) also shows a separate maximum

in the Irminger Sea (their CFC maximum is farther to the northeast than the PV minimum in Fig. 13a).

Does the Irminger PV extremum appear in the overall climatology? In answering this one must be careful that the WOCE period, which included numerous cruises during high-NAO conditions, does not bias the results. Therefore, we constructed separate climatologies with and without the WOCE period data (where pre-WOCE is prior to 1989, winter data included). Both climatologies produced comparable results, indicating that there is no appreciable biasing due to the recent data. The full climatological lateral distribution of PV (Fig. 13b) shows a weaker but significant minimum in the same area of the southwestern Irminger Sea. Note that in Fig. 13b we have displayed the 750 m surface; this is because the pre-WOCE climatology has no discernible LSW signal at 1000 m, in either basin, presumably because of the impact of low convection periods in the extensive database. The reader should note the location of the two Ocean Weather Stations in relation to the PV extremum in each sea. This shows quite graphically why convection was observed at BRAVO but not ALPHA.

These results indicate that the LSW spreading pattern of Talley and McCartney (1982) is not representative. Instead, the dominant pattern shows two distinct low PV sources, one in the Labrador Sea, and a weaker source in the Irminger Sea. Fig. 13a reveals that at times, for example, during an extended period of high NAO, the Irminger Sea source can be as strong as that in the Labrador Sea. It should be noted, however, that we are not advocating that LSW is always formed just at these two locations. For example, the April 1991 R/V *Endeavor* data set discussed above included two stations in the southeastern Labrador Sea, near the “dividing line” between the two seas, showing clear evidence of local overturning (see Pickart et al., 1997). In 1935 the Meteor data contained comparable evidence in this same area (Wattenberg, 1938; Wust, 1943). Additionally, PALACE float data from the Deep Convection Experiment showed a region of fairly deep winter mixed-layers in the eastern Labrador Sea (Lavender, 2001). Therefore, the overall impression we

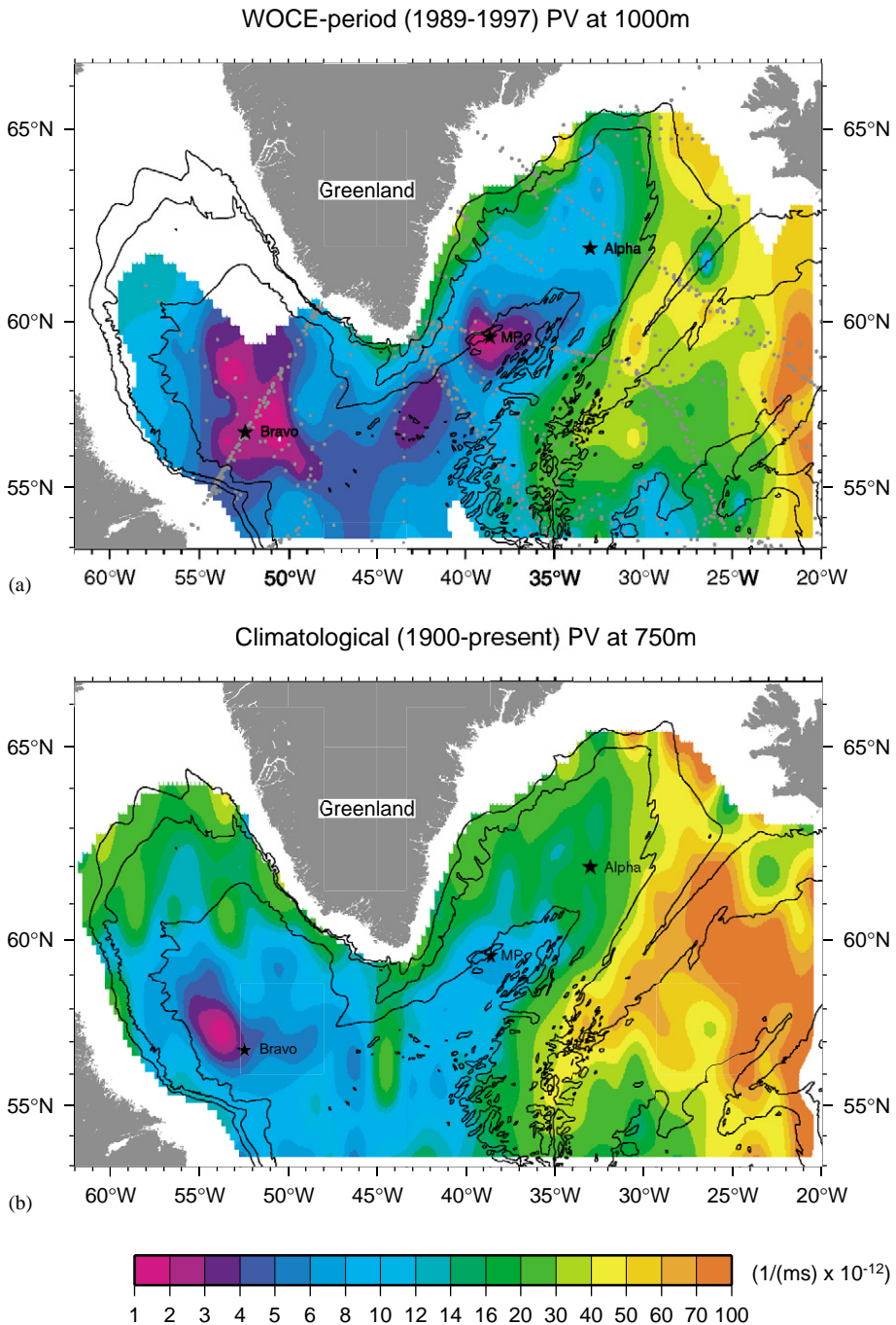


Fig. 13. Map of planetary potential vorticity (PV) based on the HydroBase 2 climatology. Ocean Weather Stations BRAVO and ALPHA are marked by stars, as well as the site of the moored CTD profiler (MP) deployed in August, 2001. The isobaths are 1000, 2000, and 3000 m. (a) PV during the recent WOCE period (stations are marked by grey dots); (b) long-term climatological PV.

wish to convey is that, although deep convection seems most predisposed to occur in the two locations in Fig. 13—one in the lee of Labrador and the other in the lee of Greenland—under strong enough forcing convection may also occur in the region between these two features.

#### 4.2. *Advective–diffusive model*

We return now to the circulation in the two seas, in particular the local cyclonic gyres on the western sides of each basin. The high-resolution view offered in Fig. 9 demonstrates that the LSW of strongest convective origin is found within the troughs of these gyres. This is supported by the lower resolution view of the climatology. Thus, the tracer fields constitute further evidence that the most weakly stratified LSW in the Irminger Basin did not emanate from the Labrador Sea via a rapid advective link. Such a link would require that the water escape the Labrador Sea gyre, flow into the Irminger Sea, then penetrate the gyre there, all within a timescale of months. Furthermore, this would not lead to the extremum of LSW properties found in the western Irminger Sea.

To investigate these issues further, we implemented an advective–diffusive numerical model using the Lavender et al. (2000) mean flow field at 700 m (the circulation of Fig. 9). Specifically, the mean flow was adjusted to make it non-divergent, then a spatially varying diffusivity was added, derived from the PALACE float variance field. Straneo et al. (in press) discuss the model in detail and use it to study water mass distributions and pathways in the western subpolar gyre. For the purposes of our study, to investigate the movement of LSW from the Labrador Sea to the Irminger Sea, we released a patch of passive tracer in the western part of the Labrador basin. This is meant to mimic the body of LSW formed there during the winter convective season; for example, the tracer can be thought of as CFCs mixed into the water column during overturning. We consider both a low-NAO (weak to moderate convection) and high-NAO (strong convection) scenario, the only difference being in the size of the initial tracer patch. For the low-NAO case a relatively small area is used, corresponding to the region of deep

mixed-layers in Fig. 9 observed during the 1997 wintertime hydrographic survey of Pickart et al. (2002a). For the high-NAO case the area was estimated by allowing the mixed-layers to continue to deepen for an additional 2 weeks beyond the time of the survey, using a deepening rate computed from a repeat occupation of one of the sections. This extrapolation resulted in a larger area of deep mixed-layers, which was taken as the region of tracer release for the high-NAO case. By presenting results for both NAO scenarios, we cover the range of possibilities for the spreading of LSW.

Because of the uncertainty in the definition of an eddy diffusivity ( $\kappa$ ), we present three different runs so as to test the sensitivity of our results to the absolute value of  $\kappa$ . The three runs are an advective case, an intermediate case (called the basic run), and a diffusive case. The diffusivity in the basic case is assumed to be directly proportional to the rms eddy float velocity, using a constant Lagrangian length scale of 20 km (see Straneo et al., in press). Therefore, the eddy diffusivity is spatially inhomogeneous in the basic simulation, with an average value of  $0.65 \times 10^7 \text{ cm}^2/\text{s}$  over the Labrador basin. The advective run ( $0.1 \times 10^7 \text{ cm}^2/\text{s}$ ) and diffusive run ( $1 \times 10^7 \text{ cm}^2/\text{s}$ ) are meant to represent the lower and upper extremes in the range of  $\kappa$ . In these cases the diffusivity is taken to be spatially uniform, which, as discussed in Straneo et al. (in press), does not affect the results for these two limits.

We use the advective–diffusive model to address two questions: How long does it take tracer, initially released in the Labrador Sea, to reach the Irminger Sea? Then, once it reaches the Irminger Sea, what kind of tracer distribution would one expect to see across the basin (e.g. along the  $\sim$ A1E section)? We show first the evolution of tracer for the high and low convection scenarios in the basic model set up (Fig. 14). One sees that the model is able to reproduce the three LSW spreading pathways described in Section 2 (Fig. 1), which are present in both scenarios.<sup>5</sup>

<sup>5</sup>The North Atlantic Current pathway is less evident than the other two, likely because this current is not well resolved in the model flow field (see Straneo et al., in press).

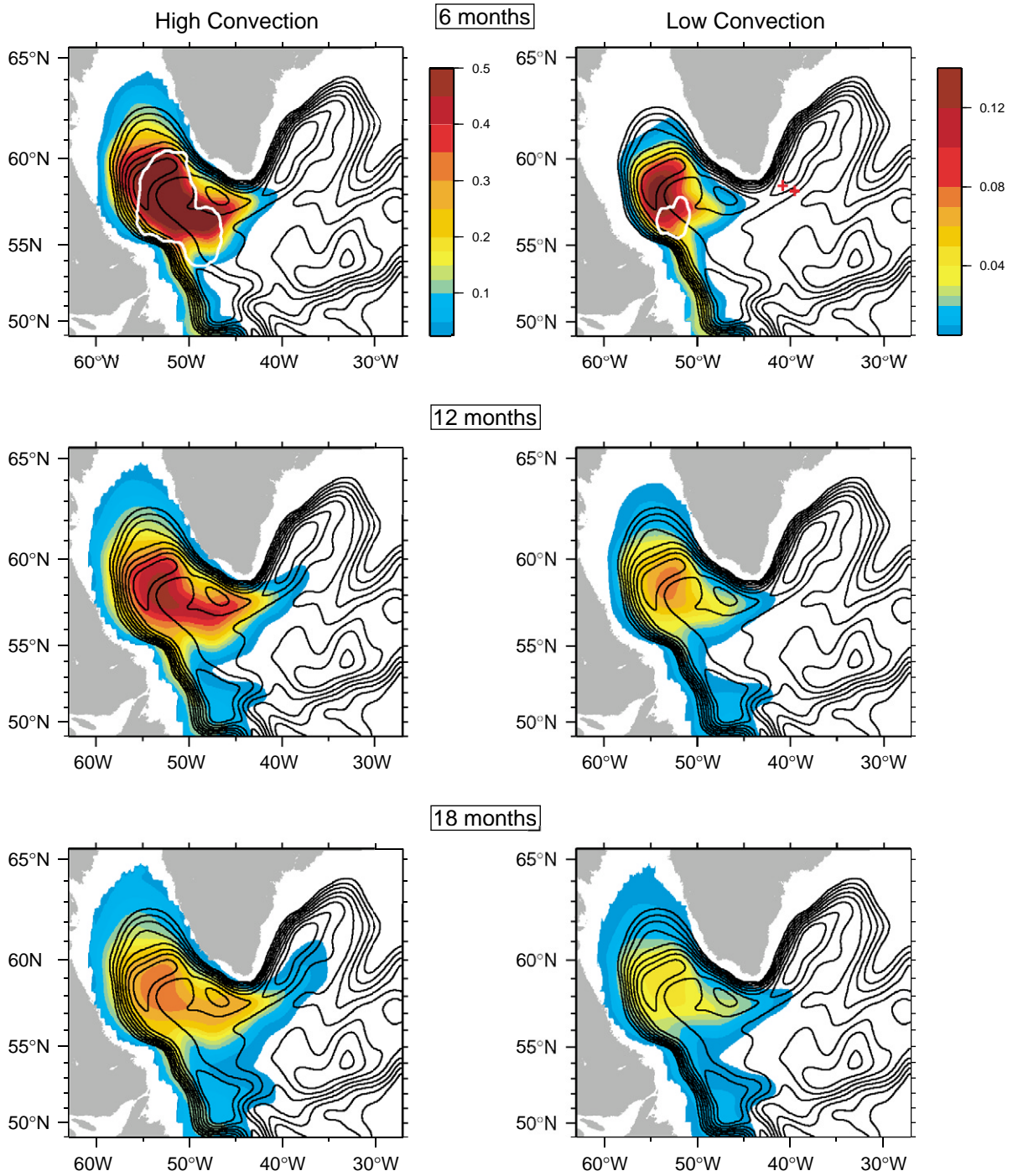


Fig. 14. Spreading of tracer in the basic model configuration, for the high (left panels) and low (right panels) convection scenario. Black contours denote the streamlines, and the white line indicates the area of initial tracer release. The two red crosses mark the Irminger gyre “center” and “edge” points along the  $\sim$ A1E line discussed in the subsequent figures.

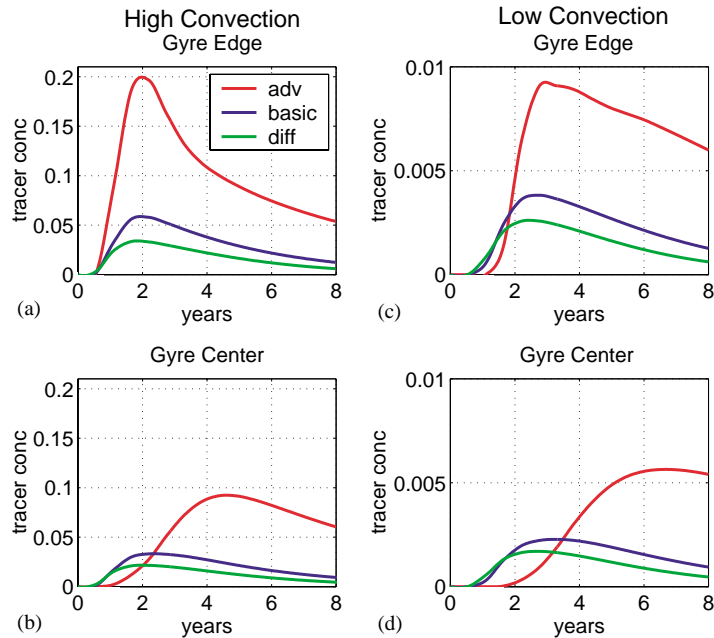


Fig. 15. Time series of tracer concentration for the three experiments, for the high convection ((a) and (b)) and low convection ((c) and (d)) cases. Time series are measured at the edge and center of the Irminger gyre (see Fig. 14).

Differences between the two cases are mostly due to the more rapid dilution of tracer in the low convection scenario (due to the initially smaller amount of tracer), and to the different areas over which tracer is initialized. Thus, there is an approximate half-year delay in the arrival of tracer to the Irminger Sea in the low versus high convection scenario, due to differences in the length of the transit path.

#### 4.2.1. Time evolution

We now present a quantitative estimate of how long it takes tracer to reach the Irminger Sea. For a single tracer release in the Labrador Sea we do this by monitoring the concentration at two locations along the  $\sim$ A1E line, one at the center of the Irminger gyre and one at the edge. These are marked in Fig. 14 (recall that the  $\sim$ A1E line is the composite Irminger Sea section in Fig. 4a). The edge of the gyre is defined as that location where the tracer is a maximum (see Fig. 17), which is common to all runs. In practice it coincides with the most direct advective pathway into the

Irminger Sea. The time series at the two locations, for both convection scenarios, are shown in Fig. 15. In both cases the arrival of tracer at the edge of the gyre is nearly independent of the diffusivity (roughly 1.8–2.0 yr in the high convection scenario, and 2.4–2.6 yr in the low convection scenario). Hence, this pathway is almost purely advective (the decrease in amplitude with increasing diffusivity is associated with a broader peak, see Fig. 17). By contrast, tracer arrival at the interior of the gyre is strongly controlled by the lateral mixing: the higher the diffusivity, the faster the peak reaches the gyre's center. In this case the arrival time ranges from 1.8 yr (high diffusion, strong convection) to > 6 yr (low diffusion, weak convection).

Tracking a one-time tracer release in this manner is somewhat artificial, however, since convection typically occurs over multiple winters. Thus, a remotely observed signal will reflect the cumulative effects of repeated convection events. As a second way of computing the LSW transit time, we computed the time it takes for a

time-varying signal to propagate from the Labrador basin to the Irminger basin. Without loss of generality, we consider a 4 yr cycle of convection, such that tracer is initialized in the Labrador Sea according to a simple sine-function evolution with this period. Specifically, the area over which the tracer is released expands and contracts between the high- and the low-NAO limits over a 4 yr cycle. Note that we ignore any preconditioning in the Labrador Sea, in that the extent of convection (tracer release) each winter is not impacted by the distribution of tracer at the end of the previous fall.

Because the advective–diffusive model is linear, periodic forcing at the source generates a periodic response downstream. Hence by comparing the lag between maxima, one can deduce the propagation time from the Labrador to the Irminger Sea. The computed arrival time of LSW is shown in Fig. 16 as a function of diffusivity for the gyre edge and center. Not surprisingly, in light of the above results for a single tracer release, the time for the signal to reach the edge of the gyre is only marginally dependent on  $\kappa$  (roughly 2–2.3 yr). In order to reduce this to the 6 month advective time suggested by Sy et al. (1997), the interior velocity would have to be increased by a factor of four (and significantly more so for the 2.5 month advective time implied by the April data presented earlier). We deem this highly unrealistic. At the center of

the gyre the arrival time does vary with diffusivity—ranging from 2 yr (high diffusivity) to 5 yr (low diffusivity). In summary, the model predicts that the shortest time for LSW to reach the Irminger Sea is 2+ years at the edge of the gyre, and up to a year longer at the center of the gyre.

#### 4.2.2. Spatial pattern

We consider now the second question: What is the expected tracer distribution along the  $\sim$ A1E section? Fig. 14 shows that as tracer enters the Irminger Sea it starts to wrap around the cyclonic gyre, and in order to reach the center of the gyre it must get mixed in via eddies. In order to compare the model results with the PV distribution of Fig. 9, we show the tracer concentration across the  $\sim$ A1E line in the model two years after tracer was released in a high convection scenario (Fig. 17). For all three runs it is seen that the maximum in concentration is located at the southeastern side of the recirculation gyre, not in the gyre's center, where the streamfunction is a minimum. Hence, even in the highly diffusive limit, the model is unable to produce the extremum of LSW properties observed in the center of the Irminger gyre.

#### 4.2.3. Slow advection

In presenting these results we are not claiming that advection of LSW from the Labrador Sea to

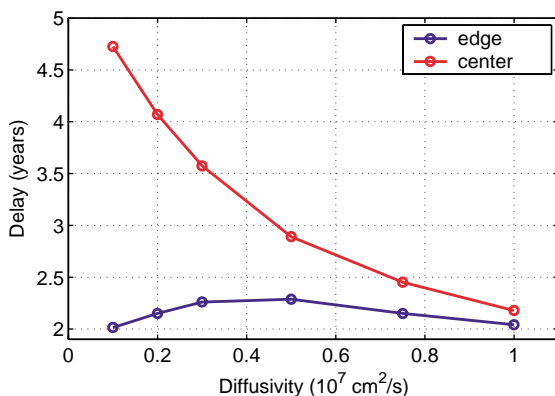


Fig. 16. Elapsed time for a tracer signal to arrive from the Labrador Sea to the edge (blue) and center (red) of the Irminger Sea gyre, as a function of diffusivity.

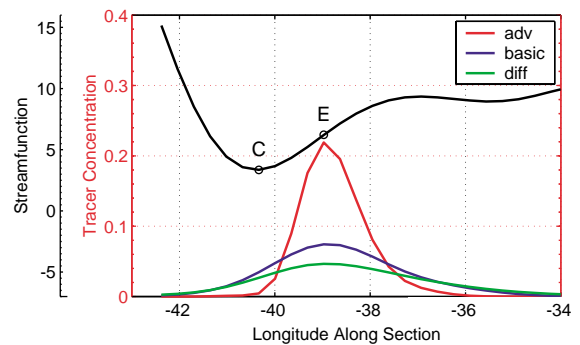


Fig. 17. Tracer concentration along the  $\sim$ A1E line after 2 yr, for the three model experiments, shown in relation to the streamfunction (black line) along the  $\sim$ A1E line. The edge and center of the Irminger gyre, discussed in Figs. 15 and 16, are denoted by the points E and C, respectively.

the Irminger Sea is unimportant. We believe such advection—albeit at a slower rate—contributes significantly to the LSW found east of Greenland. Recall the time series of LSW salinity in the two basins (Fig. 6), and the fact that they did not track each other in the latter half of the record. In light of the numerical model results, this is explainable by remote advection. After 1995, the LSW in the Labrador basin became progressively saltier. This is when the NAO index dropped precipitously (Fig. 2), and convective renewal at these depths ceased to occur (Yashayaev et al., 2000). Therefore, the salinification of the LSW in the Labrador basin is clearly the result of restratification due to salty water from the boundary current system mixing laterally into the basin. Now if local formation were the sole source of the LSW in the Irminger basin, then the same trend should have occurred there, since the salty Irminger current encircles the edge of this basin as well. However, the water in the Irminger basin continued to freshen after 1995. This is likely due to the influence of LSW arriving from the Labrador basin—formed earlier in the decade when the NAO first rose—which was significantly fresher. Arrival of this water would keep the Irminger Sea salinity from increasing. This is consistent with the timing predicted by the model, whereby it takes a few years for the water from the Labrador Sea to start influencing the center of the Irminger gyre. Therefore, we argue here as well against an Irminger Sea-centric viewpoint. Rather, both local and remote processes seem to be at work.

## 5. Concluding remarks

The prevailing notion in the modern day oceanographic literature is that deep convection in the western subpolar North Atlantic occurs exclusively in the Labrador Sea, and that this is the sole source of Labrador Sea Water (LSW). We have cast doubt on this “Labrador Sea-centric” viewpoint, showing that the existing tracer observations in the western North Atlantic cannot be explained by a Labrador-only source, and that there is compelling evidence that deep convection

occurs in the western Irminger Sea. This idea is in fact not new; it was hypothesized in the early 20th century, and even verified to some degree by wintertime observations in the 1930s. Using recently collected data, our aim has been to rekindle this notion.

If the Labrador Sea-centric viewpoint is correct, measurements presented here show that there would be an extremely short transit time for LSW to reach the Irminger basin during high-NAO conditions—less than 3 months. This implies an advective speed of 13 cm/s, which is quite unrealistic for an interior pathway. Furthermore, recent measurements during the WOCE period, as well as a 100 yr climatology, indicate that there is an extremum of LSW properties in the southwestern Irminger Sea, with values of potential vorticity that are at times as low as those found in the western Labrador Sea. This tracer distribution—two distinct extrema in the Labrador and Irminger Seas—cannot result from a single source. This was verified using an advective–diffusive numerical model which simulates the Labrador Sea-only source. The model quantified the discrepancy in the lateral distribution and timing of LSW observed in the Irminger Sea. A third discrepancy involves the dissimilar nature of the time series of LSW properties in the two seas, constructed using recent hydrographic sections.

As an alternative hypothesis for the presence of newly ventilated LSW in the Irminger Sea, we have presented evidence—albeit indirect—that convection occurs east of Greenland. It was demonstrated that the oceanographic and atmospheric conditions which result in convective overturning are nearly the same in the two seas. This includes the preconditioning of the water column, the presence of cyclonic circulation, and the atmospheric buoyancy forcing. Regarding the first two, there is nothing unique about the Labrador Sea, since the trapping of water and stratification within the gyre is the same in the Irminger Sea. Regarding the atmospheric forcing, synoptic storms influence the Irminger Sea in similar fashion to the Labrador Sea. While the resulting heat fluxes are stronger in the Labrador Sea (although this is subject to debate due to shortcomings in the global meteorological products), a

mixed-layer model shows that convection can extend to 1500–2000 m in the Irminger Sea.

Formation of LSW in the Irminger Basin carries strong ramifications. It means that there is another location where deep convection allows the atmosphere to communicate directly with the mid-depth ocean, and that there is a second contribution to the meridional overturning system in the subpolar North Atlantic. This will influence our thinking regarding various aspects of the North Atlantic subpolar gyre, including water mass transformation, circulation, spreading of tracers, and new water production rates. To verify the hypothesis presented here, direct wintertime observations of the mixed-layer in the Irminger Sea are required, preferably with concurrent meteorological measurements. It is also clear that such data need to be collected during high-NAO conditions. As a first step towards this, a moored CTD profiler has been deployed in the Irminger Sea in the region of the potential vorticity minimum (see Fig. 13). It is hoped that the resulting time series will demonstrate unequivocally whether or not deep convection, and hence LSW formation, occurs in the Irminger Sea.

### Acknowledgements

The authors are indebted to the group of investigators listed in Table 1, who kindly shared their data. We thank Kara Lavender for the use of the PALACE velocity data. Mike Spall gave us many insightful comments during the study, and Ruth Curry provided much assistance in the use of the HydroBase 2 climatology. RP was funded under grants N00014-97-1-0043 from the Office of Naval Research, and OCE-0002492 from the National Science Foundation.

### References

- Bumke, K., Karger, U., Uhlig, K., 2002. Measurements of turbulent fluxes of momentum and sensible heat over the Labrador Sea. *Journal of Physical Oceanography* 32, 401–410.
- Clarke, R.A., Coote, A.R., 1988. The formation of Labrador Sea water. Part III: the evolution of oxygen and nutrient concentration. *Journal of Physical Oceanography* 18, 469–480.
- Clarke, R.A., Gascard, J.C., 1983. The formation of Labrador Sea water. Part I: large-scale processes. *Journal of Physical Oceanography* 33, 1764–1778.
- Cunningham, S.A., Haine, T.W.N., 1995. Labrador Sea water in the eastern North Atlantic. Part I: a synoptic circulation inferred from a minimum in potential vorticity. *Journal of Physical Oceanography* 25, 649–665.
- Curry, R.G., 1996. HydroBase: a database of hydrographic stations and tools for climatological analysis. Technical Report WHOI-96-01, Woods Hole Oceanographic Institution, 44 pp.
- Curry, R.G., 2002. What happened to the Florida Current? A comparison of climatology products. *Geophysical Research Letters*, submitted for publication.
- DeCosmo, J., Katsaros, K.B., Smith, S.D., Anderson, R.J., Oost, W.A., Bumke, K., Chadwick, H., 1996. Air–sea exchange of water vapor and sensible heat: the Humidity Exchange over the Sea (HEXOS) results. *Journal of Geophysical Research* 101, 12,001–12,016.
- Defant, A., 1936. Bericht über die ozeanographischen Untersuchungen des Vermessungsschiffes “Meteor” in der Denemarkstrasse und in der Irmingersee. *Sitzungsberichte der Preussischen Akademie der Wissenschaften. Physikalisch-Mathematische Klasse XIX*, 232–242.
- Dickson, R.R., Lazier, J.R.N., Meincke, J., Rhines, P.B., Swift, J., 1996. Long-term coordinated changes in the convective activity of the North Atlantic. *Progress in Oceanography* 38, 241–295.
- Dickson, R.R., Yashayaev, I., Meincke, J., Turrell, B., Dye, S., Holfort, J., 2002. Rapid freshening of the deep North Atlantic over the past four decades. *Nature* 416, 832–837.
- Doyle, J.D., Shapiro, M.A., 1999. Flow response to large-scale topography: the Greenland tip jet. *Tellus* 51, 728–748.
- Ellett, D.J., 1993. Transit times to the NE Atlantic of Labrador sea water signals. *International Council for the Exploration of the Sea C.M. 1993/C:25*, pp. 1–11.
- Harvey, J., Arhan, M., 1988. The water masses of the central North Atlantic in 1983–1984. *Journal of Physical Oceanography* 18, 1855–1875.
- Hurrell, J.W., 1995. Decadal trends in the North Atlantic Oscillation regional temperatures and precipitation. *Science* 269, 676–679.
- Koltermann, K.P., Sokov, A.V., Tereschenkov, V.P., Dobroliubov, S.A., Lorbacher, K., Sy, A., 1999. Decadal changes in the thermohaline circulation of the North Atlantic. *Deep-Sea Research I* 46, 109–138.
- Labsea Group, 1998. The Labrador Sea Deep Convection Experiment. *Bulletin of the American Meteorological Society* 79, 2033–2058.
- Lavender, K.L., 2001. The general circulation and open-ocean deep convection in the Labrador Sea: a study using subsurface floats. Ph.D. Thesis, University of California, San Diego. Scripps Institution of Oceanography, 131pp.
- Lavender, K.L., Davis, R.E., Owens, W.B., 2000. Mid-depth recirculation observed in the interior Labrador and

- Irminger Seas by direct velocity measurements. *Nature* 407, 66–69.
- Lazier, J.R.N., 1973. The renewal of Labrador Sea water. *Deep-Sea Research* 20, 341–353.
- Lazier, J.R.N., 1980. Oceanographic conditions at Ocean Weather Ship BRAVO, 1964–1974. *Atmosphere-Ocean* 3, 227–238.
- Lazier, J.R.N., Wright, D.G., 1993. Annual velocity variations in the Labrador Current. *Journal of Physical Oceanography* 23, 559–678.
- Lazier, J.R.N., Clarke, A., Yashayaev, I., Rhines, P., 2002. Convection and restratification in the Labrador Sea, 1990–2000. *Journal of Physical Oceanography*, in press.
- Lilly, J.M., Rhines, P.B., Visbeck, M., Davis, R., Lazier, J.R.N., Schott, F., Farmer, D., 1999. Observing deep convection in the Labrador Sea during winter 1994/95. *Journal of Physical Oceanography* 29, 2065–2098.
- Marshall, J., Schott, F., 1999. Open-ocean convection: observations, theory, and models. *Reviews of Geophysics* 37, 1–64.
- McCartney, M.S., 1992. Recirculating components to the deep boundary current of the northern North Atlantic. *Progress in Oceanography* 29, 283–383.
- McCartney, M.S., Talley, L.D., 1982. The subpolar mode water of the North Atlantic Ocean. *Journal of Physical Oceanography* 12, 1169–1188.
- MEDOC GROUP, 1970. Observation of formation of deep water in the Mediterranean Sea, 1969. *Nature* 227, 1037–1040.
- Moore, G.W.K., Renfrew, I.A., 2002. An assessment of the surface turbulent heat fluxes from the NCEP-NCAR reanalysis over the western boundary currents. *Journal of Climate* 15, 2020–2037.
- Nansen, F., 1912. Das bodenwasser und die abkühlung des meeres. *Internationale Revue der gesamten Hydrobiologie und Hydrographie Band V* (1), 1–42.
- Nielsen, J., 1928. The waters around Greenland. In: Vahl, M. (Ed.), *Greenland, The Discovery of Greenland, Exploration, and the Nature of the Country, Vol. I*. Oxford University Press, Oxford, pp. 185–230.
- Pagowski, M., Moore, G.W.K., 2001. A numerical study of an extreme cold-air outbreak over the Labrador Sea: sea–ice air–sea interaction and the development of polar lows. *Monthly Weather Review* 129, 47–72.
- Pickart, R.S., Smethie Jr., W.M., 1998. Temporal evolution of the Deep Western Boundary Current where it enters the sub-tropical domain. *Deep-Sea Research I* 45, 1053–1083.
- Pickart, R.S., Spall, M.A., Lazier, J.R.N., 1997. Mid-depth ventilation in the western boundary current system of the sub-polar gyre. *Deep-Sea Research I* 44, 1025–1054.
- Pickart, R.S., Torres, D.J., Clarke, R.A., 2002a. Hydrography of the Labrador Sea during active convection. *Journal of Physical Oceanography* 32, 428–457.
- Pickart, R.S., Spall, M.A., Ribergaard, M.H., Moore, G.W.K., Milliff, R.F., 2002b. Deep Convection east of Greenland: atmospheric forcing and oceanic response. *Nature*, submitted for publication.
- Read, J.F., Gould, W.J., 1992. Cooling and freshening of the sub-polar North Atlantic ocean since the 1960's. *Nature* 360, 55–57.
- Renfrew, I.A., Holt, T.R., Chang, S.W., Guest, P., 1999. Meso-scale forecasting during a field program: meteorological support of the Labrador Sea Convection Experiment. *Bulletin of American Meteorological Society* 80, 605–620.
- Renfrew, I.A., Moore, G.W.K., Guest, P.S., Bumke, K., 2002. A comparison of surface-layer heat flux and surface momentum flux observations over the Labrador Sea with ECMWF analyses and NCEP reanalyses. *Journal of Physical Oceanography* 32, 383–400.
- Rhein, M., Fischer, J., Smethie Jr., W.M., Smythe-wright, D., Weiss, R.F., Mertens, C., Min, D.H., Fleischmann, U., Putzka, A., 2002. Labrador Sea water: pathways, CFC-inventory, and formation rates. *Journal of Physical Oceanography* 32, 648–665.
- Rogers, J.C., 1990. Patterns of low-frequency monthly sea level pressure variability (1899–1986) and associated wave cyclone frequencies. *Journal of Climate* 3, 1364–1379.
- Schmitz, W.J., McCartney, M.S., 1993. On the North Atlantic circulation. *Reviews of Geophysics* 31, 29–49.
- Smethie Jr., W.M., Fine, R.A., 2000. Rates of North Atlantic deep water formation calculated from chlorofluorocarbon inventories. *Deep-Sea Research I* 48, 189–215.
- Smethie Jr., W.M., Fine, R.A., Putzka, A., Jones, E.P., 2000. Tracing the flow of North Atlantic deep water using chlorofluorocarbons. *Journal of Geophysical Research* 105, 14,297–14,323.
- Smith, S.D., 1988. Coefficients for sea surface wind stress, heat flux, and wind profiles as a function of wind speed and temperature. *Journal of Geophysical Research* 93, 15,467–15,472.
- Spall, M.A., 1996. Dynamics of the Gulf Stream/Deep Western Boundary Current crossover. Part II: low-frequency internal oscillations. *Journal of Physical Oceanography* 26, 2169–2182.
- Spall, M.A., Pickart, R.S., 2001. Where does dense water sink? A subpolar gyre example. *Journal of Physical Oceanography* 31, 810–826.
- Spall, M.A., Pickart, R.S., 2002. Wind-driven recirculations and exchange in the Labrador and Irminger Seas. *Journal of Physical Oceanography*, accepted for publication.
- Speer, K.G., Isemer, H.-J., Biastoch, A., 1995. Water mass formation from revised COADS data. *Journal of Physical Oceanography* 25, 2444–2457.
- Straneo, F., Pickart, R.S., Lavender, K.L. Spreading of Labrador Sea water: an advective–diffusive study based on Lagrangian data. *Deep-Sea Research I*, in press.
- Sy, A., Rhein, M., Lazier, J.R.N., Koltermann, K.P., Meincke, J., Putzka, A., Bersch, M., 1997. Surprisingly rapid spreading of newly formed intermediate waters across the North Atlantic Ocean. *Nature* 386, 675–679.
- Talley, L.D., 1999. Mode waters in the subpolar North Atlantic in historical data and during the WOCE period. *International WOCE Newsletter* 37, 3–6.

- Talley, L.D., 2000. The shallow, intermediate and deep overturning components of the global heat budget. EOS, Transactions, American Geophysical Union 80, OS52.
- Talley, L.D., McCartney, M.S., 1982. Distribution and circulation of Labrador Sea Water. *Journal of Physical Oceanography* 12, 1189–1205.
- Top, Z., Clarke, W.B., Jenkins, W.J., 1987. Tritium and primordial  $^3\text{He}$  in the North Atlantic: a study in the region of the Charlie-Gibbs Fracture Zone. *Deep-Sea Research I* 34, 287–298.
- Wallace, D.W.R., Lazier, J.R.N., 1988. Anthropogenic Chlorofluorocarbons in newly-formed Labrador Sea Water. *Nature* 332, 61–63.
- Wattenberg, H., 1938. Die Verteilung des sauerstoffs im Atlantischen Ozean. Verlag Von Walter de Gruyter & Co., Berlin, 132pp.
- Weiss, R.F., Bullister, J.L., Gammon, R.H., Warner, M.J., 1985. Atmospheric chlorofluoromethanes in the deep equatorial Atlantic. *Nature* 314, 608–610.
- Worthington, L.V., 1976. On the North Atlantic circulation. *The Johns Hopkins Oceanographic Studies* 6, 110pp.
- Wright, W.R., 1972. Northern sources of energy for the deep Atlantic. *Deep-Sea Research* 19, 865–877.
- Wüst, G., 1943. Der subarktische bodenstrom in der westatlantischen mulde. *Annanlen der Hydrographie und Maritimen Meteorologie Heft IV/VI*, 249–256.
- Yashayaev, I.M., Clarke, R.A., Lazier, J.R.N., 2000. Recent decline of the Labrador Sea Water. *International Council for the Exploration of the Sea CM*, 2000/L:18, 10pp.